

# A Search for the Lepton Flavor Violation Decays $B_{s,d}^0 \rightarrow e^+ \mu^-$

Kaori Maeshima, Ting Miao, Hans Wenzel

*Fermilab*

## Abstract

The decays  $B_s^0 \rightarrow e^+ \mu^-$  and  $B_d^0 \rightarrow e^+ \mu^-$  are forbidden in the Standard Model by lepton number conservation. They can occur, however, in some extensions of the Standard Model, such as the Pati-Salam model or some SUSY models. The Pati-Salam model, for example, predicts the existence of a new type of gauge boson, called leptoquark, to mediate these decays. The value of the leptoquark mass is directly related to the decay branching ratios for these decays. With  $2 \text{ fb}^{-1}$  CDF data collected by the two-track SVT trigger, we perform a direct search for these decays. We find one event in the  $B_s^0 \rightarrow e^+ \mu^-$  mass window with estimated  $0.81 \pm 0.63$  background events and two events in the  $B_d^0 \rightarrow e^+ \mu^-$  mass window with estimated  $0.94 \pm 0.63$  background events. Using candidate  $B_d^0 \rightarrow K^+ \pi^-$  events collected with the same trigger path for a relative normalization, we derive the limits on the decay branching ratios  $Br(B_s^0 \rightarrow e^+ \mu^-) < 2.0(2.6) \times 10^{-7}$  and  $Br(B_d^0 \rightarrow e^+ \mu^-) < 6.4(7.9) \times 10^{-8}$  at 90(95)% confidence level. The corresponding lower bounds on the Pati-Salam leptoquark mass are  $M_{LQ}(B_s^0) > 47.7(44.6) \text{ TeV}/c^2$  for the  $B_s^0$  and  $M_{LQ}(B_d^0) > 58.6(55.7) \text{ TeV}/c^2$  for the  $B_d^0$  at 90 (95)% confidence level.

We also performed a search for the flavor changing neutral current decays  $B_{s,d}^0 \rightarrow e^+ e^-$ . We obtain  $Br(B_s^0 \rightarrow e^+ e^-) < 2.8(3.7) \times 10^{-7}$  and  $Br(B_d^0 \rightarrow e^+ e^-) < 8.3(10.6) \times 10^{-8}$  at 90 (95)% confidence level. This is the first time a limit is set on the decay branching ratio of  $B_s^0 \rightarrow e^+ e^-$ .

# Contents

1	Introduction	3
2	The data sample and event selection	7
3	Electron and muon identification	9
4	Measurement Optimization	13
5	Search Windows and Event Counting	22
6	Relative Efficiency and Acceptance	27
7	Limits on the branching ratios and Leptoquark masses	30
8	Search for the decays $B_{s,d}^0 \rightarrow e^+e^-$	33
9	Summary	37

# 1 Introduction

The decays  $B_{s,d}^0 \rightarrow e^+\mu^-$  are strictly forbidden within the standard model of electroweak interaction.<sup>1</sup> These decays are allowed, however, in some extensions to the standard model, such as Pati-Salam model [1] or some super symmetry (SUSY) model [2], with the assumption of a local gauge symmetry between quarks and leptons leads to the prediction of a new force of nature which mediates transitions between quarks and leptons [3][4]. The search for these lepton flavor violation decays is thus probing physics beyond the Standard Model.

The simplest model which incorporates the idea of quark and lepton symmetry is the Pati-Salam model [1] based on the group  $SU(4)_c$  where the lepton number is the fourth "color". At some high-energy scale, the group  $SU(4)_c$  is spontaneously broken to  $SU(3)_c$ , liberating the leptons from the influence of the strong interaction and breaking the symmetry between quarks and leptons. This model predicts a heavy spin one gauge boson with non-chiral couplings to quarks and leptons called Pati-Salam leptoquark - an exotic particle carrying color as well as leptonic quantum numbers. S. Willenbrock and G. Valencia point out [3] that theoretically the lepton and quark components in a leptoquark are not necessarily from the same generation. They also state that rare  $K, \pi$ , and  $B$  meson decays are the most sensitive probes for quark-lepton transitions mediated by heavy Pati-Salam leptoquarks. The decay  $B_s^0 \rightarrow e^+\mu^-$  shown in Figure 1 probes two types: (1) a leptoquark which relates the first generation lepton with the third generation quark and the second generation lepton with the second generation quark, (2) a leptoquark which relates the first generation lepton with the second generation quark and the second generation lepton with the third generation quark.<sup>2</sup>

Within the Pati-Salam model, the following relationship between the  $Br(B_s^0 \rightarrow e^+\mu^-)$  and the leptoquark mass ( $M_{LQ}$ ) can be derived:

$$Br(B_s^0 \rightarrow e^+\mu^-) = \Gamma(B_s^0 \rightarrow e^+\mu^-) \cdot \frac{\tau_{B_s^0}}{\hbar} = \pi\alpha_s(M_{LQ}) \frac{1}{M_{LQ}^4} F_B^2 m_B^3 R^2 \cdot \frac{\tau_{B_s^0}}{\hbar} \quad (1)$$

where  $R = \frac{m_{B_s}}{m_b} \left( \frac{\alpha_s(M_{LQ})}{\alpha_s(m_t)} \right)^{-\frac{4}{7}} \left( \frac{\alpha_s(m_t)}{\alpha_s(m_b)} \right)^{-\frac{12}{23}}$

The values of quantities that we used in the theoretical calculation of  $M_{LQ}$  and the uncertainties thereof are listed in Table 1. The strong coupling constant  $\alpha_s$  as a function of  $q^2$ , shown in Figure 2, is obtained using the Marciano approximation [5] with input value  $\alpha_s(M_Z^0) = 0.115$  at the  $Z^0$  mass pole assuming no colored particles lie between  $m_t$  and  $M_{LQ}$ .

---

<sup>1</sup>Through this note, charge-conjugate modes are always implied unless specified otherwise.

<sup>2</sup>Similarly, the decay  $B_d^0 \rightarrow e^+\mu^-$  shown in Figure 1 probes: (1) a leptoquark which relates the first generation lepton with the third generation quark and the second generation lepton with the first generation quark, (2) a leptoquark which relates the first generation lepton with the first generation quark and the second generation lepton with the third generation quark.

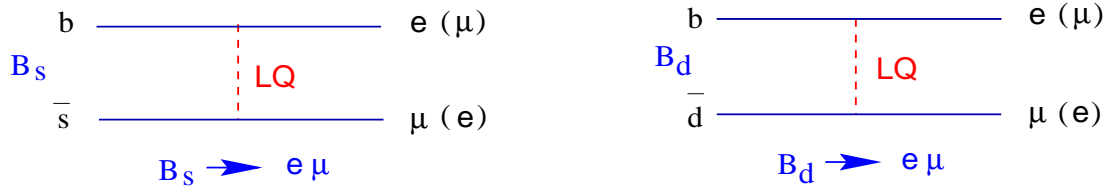


Figure 1: Feynman diagrams of  $B_s^0 \rightarrow e^+ \mu^-$  and  $B_d^0 \rightarrow e^+ \mu^-$  decays mediated by Pati-Salam leptoquarks (LQ).

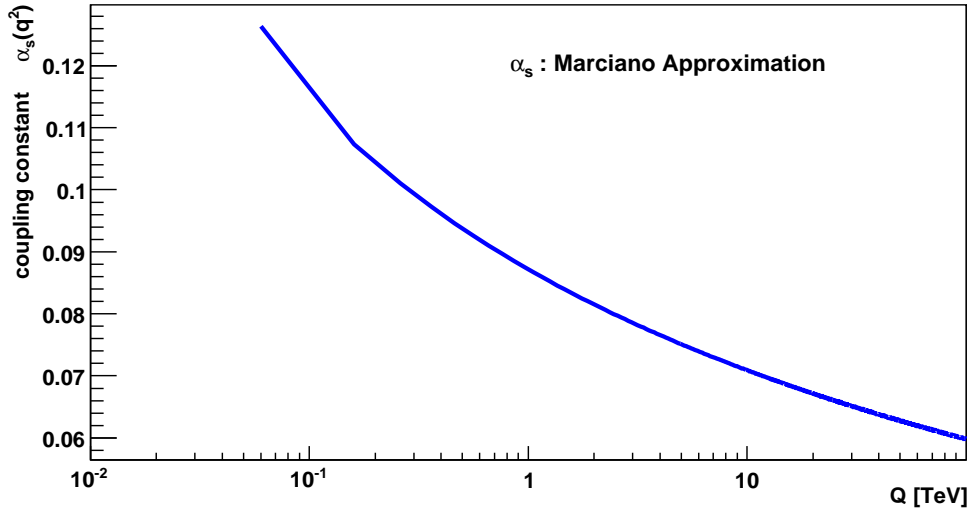


Figure 2: Strong coupling constant  $\alpha_s$  as a function of  $q^2$  using the Marciano approximation.

Table 1: Values of quantities used in the theoretical calculation of  $M_{LQ}$  and the uncertainties thereof.

Quantity	Value
top quark mass: $m_t$	$172.5 \pm 2.7$ GeV [6]
b quark mass: $m_b$	$4.2 \pm 0.07$ GeV [6]
c quark mass: $m_c$	$1.25 \pm 0.009$ GeV [6]
coupling strength: $F_{B_d}$	$0.175 \pm 0.030$ GeV
coupling strength: $F_{B_s}$	$0.200 \pm 0.035$ GeV
$B_d$ -meson mass: $m_{B_d}$	$5.27950 \pm 0.00033$ GeV [6]
$B_s$ -meson mass: $m_{B_s}$	$5.3661 \pm 0.0006$ GeV [6]
$B_d$ -meson lifetime: $\tau_{B_d}$	$1.530 \pm 0.009 \times 10^{-12}$ s [6]
$B_s$ -meson lifetime: $\tau_{B_s}$	$1.437 \pm 0.031 \times 10^{-12}$ s [6]

Figures 3 and 4 show the branching ratios  $\text{Br}(B_s^0 \rightarrow e^+\mu^-)$  and  $\text{Br}(B_d^0 \rightarrow e^+\mu^-)$  respectively as a function of the leptoquark mass. We shall use this relationships to set leptoquark mass limits from our measured  $\text{Br}(B_s^0 \rightarrow e^+\mu^-)$  and  $\text{Br}(B_d^0 \rightarrow e^+\mu^-)$  limits.

There are several experiment limits published for the  $B_d^0 \rightarrow e^+\mu^-$  decays from BABAR, BELLE, CLEO and CDF (Run-I):

$$\text{Br}(B_d^0 \rightarrow e^+\mu^-) < 9.2 \times 10^{-8} \text{ at } 90\% \text{ C.L. (BABAR) [7],}$$

$$\text{Br}(B_d^0 \rightarrow e^+\mu^-) < 1.7 \times 10^{-7} \text{ at } 90\% \text{ C.L. (BELLE) [8],}$$

$$\text{Br}(B_d^0 \rightarrow e^+\mu^-) < 1.5 \times 10^{-6} \text{ at } 90\% \text{ C.L. (CLEO2) [9] and}$$

$$\text{Br}(B_d^0 \rightarrow e^+\mu^-) < 3.5(4.5) \times 10^{-6} \text{ at } 90(95)\% \text{ C.L. (CDF) [10].}$$

To date, there is only one published experimental limit on  $\text{Br}(B_s^0 \rightarrow e\mu)$ :

$$\text{Br}(B_s^0 \rightarrow e^+\mu^-) < 6.1(8.2) \times 10^{-6} \text{ at } 90(95)\% \text{ C.L. (CDF) [10].}$$

The best limits on the mass of the corresponding Pati-Salam leptoquarks are:

$$M_{LQ}(B_d^0) > 53.1 \text{ TeV}/c^2 \text{ at } 90\% \text{ C.L. (BABAR) [7] and}$$

$$M_{LQ}(B_s^0) > 20.7(19.3) \text{ TeV}/c^2 \text{ at } 90(95)\% \text{ C.L. (CDF) [10].}$$

The CDF Run-I measurement was an absolute measurement using a electron-muon triggered sample with an integrated luminosity of  $102 \text{ pb}^{-1}$ . The branching ratio limit was calculated using the following relation:  $\text{Br}(B_{s,d}^0 \rightarrow e^+\mu^-) = N(B_{s,d}^0 \rightarrow e^+\mu^-) / [2\sigma(B_{s,d}^0) \cdot \mathcal{L}_{total} \cdot \epsilon]$ , where  $N(B_{s,d}^0 \rightarrow e^+\mu^-)$  is number of observed events,  $\sigma(B_{s,d}^0)$  is the production cross-section of  $B_{s,d}^0$ ,  $\mathcal{L}_{total}$  is the integrated luminosity and  $\epsilon$  is the detector efficiency including acceptance. The total systematic error (26%) on the limit was dominated by the cross section uncertainty (23%), while the luminosity measurement and detector efficiency contributed 8% and 10% respectively.

In Run-II, we perform a relative measurement using samples collected by the two-track SVT trigger. The reference decay mode for both  $B_s^0 \rightarrow e^+\mu^-$  and  $B_d^0 \rightarrow e^+\mu^-$  is  $B_d^0 \rightarrow K^+\pi^-$  which has a well measured branching ratio of  $19.4 \pm 0.6 \times 10^{-6}$  [11].

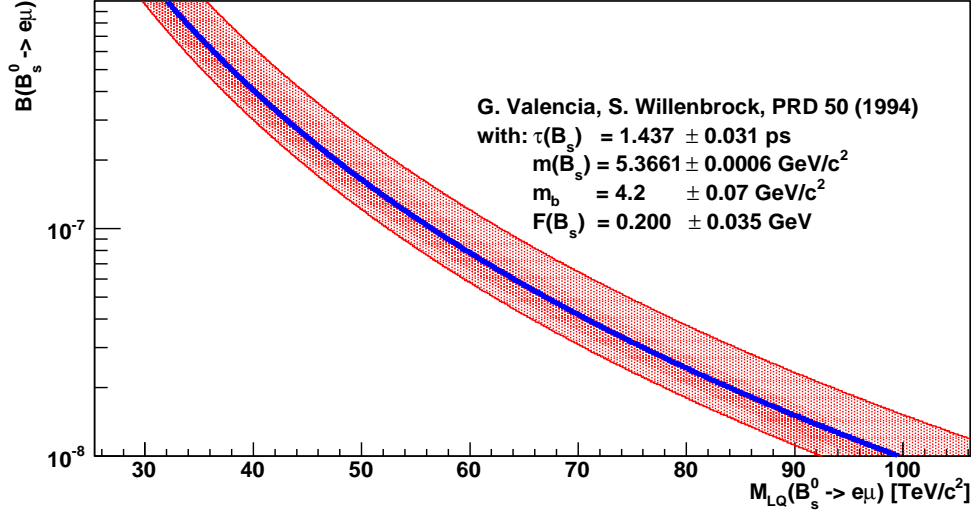


Figure 3:  $Br(B_s^0 \rightarrow e^+ \mu^-)$  as a function of the corresponding Leptoquark mass. The upper and lower curves represent theoretical uncertainties.

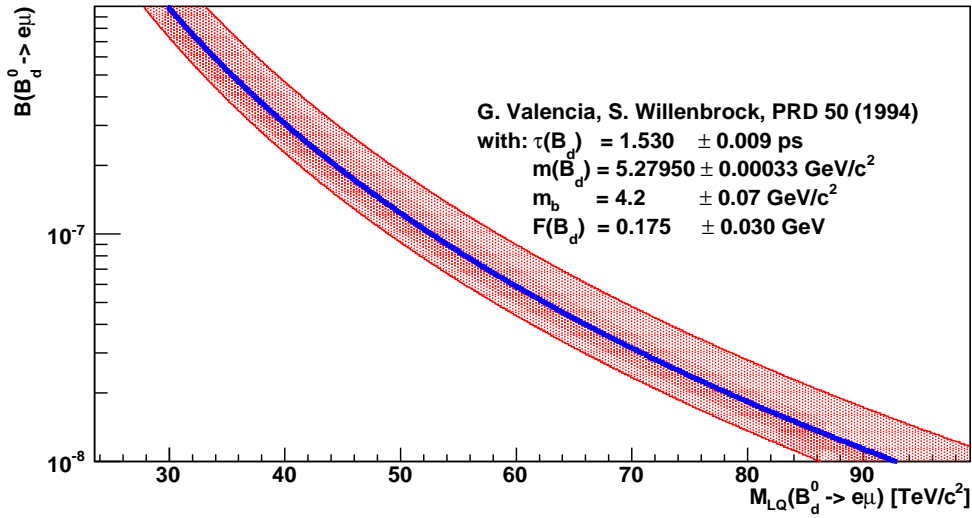


Figure 4:  $Br(B_d^0 \rightarrow e^+ \mu^-)$  as a function of the corresponding Leptoquark mass. The upper and lower curves represent theoretical uncertainties.

The branching ratios are thus calculated as:

$$Br(B_s^0 \rightarrow e^+\mu^-) = \frac{N(B_s^0 \rightarrow e^+\mu^-) \cdot Br(B_d^0 \rightarrow K^+\pi^-) \cdot f_{B_d^0}/f_{B_s^0}}{\epsilon_{B_s^0 \rightarrow e^+\mu^-}^{rel} \cdot N(B_d^0 \rightarrow K^+\pi^-)}. \quad (2)$$

$$Br(B_d^0 \rightarrow e^+\mu^-) = \frac{N(B_d^0 \rightarrow e^+\mu^-) \cdot Br(B_d^0 \rightarrow K^+\pi^-)}{\epsilon_{B_d^0 \rightarrow e^+\mu^-}^{rel} \cdot N(B_d^0 \rightarrow K^+\pi^-)}, \quad (3)$$

where  $N(B_d^0 \rightarrow e^+\mu^-)$ ,  $N(B_s^0 \rightarrow e^+\mu^-)$  and  $N(B_d^0 \rightarrow K^+\pi^-)$  are the numbers of observed candidates from  $B_d^0 \rightarrow e^+\mu^-$ ,  $B_s^0 \rightarrow e^+\mu^-$  and  $B_d^0 \rightarrow K^+\pi^-$  decays respectively;  $\epsilon_{B_d^0 \rightarrow e^+\mu^-}^{rel}$  and  $\epsilon_{B_s^0 \rightarrow e^+\mu^-}^{rel}$  are the detector acceptance and event selection efficiencies for observing  $B_d^0 \rightarrow e^+\mu^-$  and  $B_s^0 \rightarrow e^+\mu^-$  decays relative to  $B_d^0 \rightarrow K^+\pi^-$ ; and  $f_{B_d^0}/f_{B_s^0}$  [12] is the ratio of the b-quark fragmentation probabilities at the Tevatron.  $(0.398 \pm 0.012)/(0.103 \pm 0.014) = 3.86 \pm 0.59$ , where the (anti-)correlation between the uncertainties has been accounted for [12]. The uncertainty from the fragmentation fraction dominates the systematic uncertainties for the  $B_s^0 \rightarrow e^+\mu^-$  channel.

The decay  $B_s^0 \rightarrow K^+K^-$  is potentially a better choice as reference channel for  $B_s^0 \rightarrow e^+\mu^-$ . But the current measurement error of its decay branching ratio  $Br(B_s^0 \rightarrow K^+K^-)$  is much larger. In addition, the current result of  $Br(B_s^0 \rightarrow K^+K^-)$  is from the Tevatron and is suffering the same uncertainty from  $f_{B_d^0}/f_{B_s^0}$ . So we will not use the  $B_s^0 \rightarrow K^+K^-$  as a reference channel at this time.

## 2 The data sample and event selection

The data samples used in the analysis were collected by the B\_PIP1 and B\_PIP1HIGHPT trigger paths. The detailed description of the trigger paths can be found in [13]. The compressed data samples *xbpp0d*, *xbpp0h*, *xbpp0i* and *xbpp0j* with run range of 138809 - 241664 are used for this analysis. We require that the runs included are in the standard good run list for  $B_s$ -mixing like analysis (Bs=1 in the GoodRunV18.C) where good detector conditions of COT, SVX, SVT and CEM are required. In addition, runs included in this analysis are required to have good CMU and CMX detector conditions. The total integrated luminosity is about  $2fb^{-1}$  for these runs.

The off-line event reconstruction starts with the selection of a pair of good tracks with at least three SVX  $r-\phi$  hits attached to each of them. The tracks in the pair are required to have at least five associated hits each from at least two axial and two stereo COT super layers. Next the track pair is checked against the list of SVT tracks used during Level-trigger using the trigger confirmation function “BTrigUtil::pass\_TTT (track1, track2,...)” provided in the software package “BottomTools”. The explicit requirements for the trigger confirmation are listed in Table 2. In addition a positive confirmation with the trigger path is required before forming a decay vertex from the track pair. The package “CTVMFT” is used to fit the two-track vertex and track pairs with  $\chi^2 < 5$  are selected for further off-line analysis.

All candidate events for both the reference signal,  $B_d^0 \rightarrow K^+\pi^-$ , and the search channels,  $B_s^0 \rightarrow e^+\mu^-$  and  $B_d^0 \rightarrow e^+\mu^-$ , are required to pass a set of common selection cuts, shown in Table 3. These cuts confirm the trigger selection criteria off-line that were used by the  $B \rightarrow h^+h^-$  analysis [14].

Table 2: *Trigger confirmation requirements in BTrigUtil::pass\_TTT(...).*

Requirement	Value
<i>opp_charge</i>	true
<i>pt_min</i>	2.0
<i>sumpt_min</i>	5.5
<i>d0_min</i>	0.01
<i>d0_max</i>	0.1
<i>deltaphi_min</i>	0.349
<i>deltaphi_max</i>	2.356
<i>lxy_min</i>	0.02
<i>abs_lxy</i>	true
<i>ip_max</i>	0.014
<i>chi2_max</i>	25

Most of the cuts listed in Table 3 are common to various analysis in the  $B$  group and their descriptions can be found in [13] and [14]. Here we only repeat the definition and their usage of the last three cuts which turn out to be the most effective ones to reduce background for our reference and search channels.

The Isolation,  $Iso$ , of the two track pair is defined as  $Iso = p_T^B / [p_T^B + \sum p_{trk}]$  where the sum is the scalar sum of all tracks excluding the two candidate tracks within a cone of  $\Delta R < 1$  (where  $\Delta R = \sqrt{(\Delta\eta)^2 + (\Delta\phi)^2}$ ) around the momentum vector of the two track pair. In the sum of the tracks, we include only those tracks whose z-coordinate of the vertex is within 5 cm of the  $B$  candidate vertex. The pointing angle  $\Delta\phi$  is the angle between the transverse momentum vector of the reconstructed  $B$  and the vector pointing from the primary vertex to the  $B$  decay vertex.

Figure 5 shows the  $B \rightarrow h^+h^-$  invariant mass distribution after the common selection cuts have been applied. For this plot both tracks are assigned the  $\pi$  mass when calculating the invariant mass. The various curves show the different components of the sample as estimated by the fit. The fit estimates that  $13195 \pm 251$  events of 2-body B-meson ( $B_s^0$  or  $B_d^0$ ) decays,  $B_{s,d}^0 \rightarrow h^+h^-$ , where  $h^\pm$  can be a pion or Kaon.

Figure 6 shows the distributions of the transverse decay length  $L_{xy}$ , pointing angle and Isolation for  $B \rightarrow h^+h^-$  signal and background events. Here the background events are the events in the sideband region ( $5.536\text{GeV} < m_{\pi\pi} < 5.763\text{GeV}$ ). The signal distribution is obtained by sideband subtracting events in the signal region ( $5.2396\text{GeV} < m_{\pi\pi} < 5.3643\text{GeV}$ ). It shows that these three cuts are very effective

Table 3: *Common selection cuts for all B decay events.*

# axial COT SLs with $\geq 5$ hits	$\geq 2$
# stereo COT SLs with $\geq 5$ hits	$\geq 2$
# $r - \varphi$ SVXII Hits	$\geq 3$
$ \eta(1, 2) $	$\leq 1$
$p_T(1, 2)$	$\geq 2\text{GeV}/c$
$p_T(1) + p_T(2)$	$\geq 5.5\text{GeV}/c$
$q(1) \times q(2)$	$< 0$
$\Delta\phi(1, 2)$	$20^\circ < \Delta\phi < 135^\circ$
$ d_0(1, 2) $	$140\mu\text{m} <  d_0  < 1\text{mm}$
$d_0(1) * d_0(2)$	$< 0$
$ \eta(B) $	$\leq 1$
$ d_0(B) $	$\leq 80\mu\text{m}$
transverse decay length: $L_{xy}(B)$	$\geq 300\mu\text{m}$
Isolation: Iso	$\geq 0.55$
pointing angle: $\Delta\phi$	$\geq 0.12$

in reducing background. It also gives some indication of the values of the cuts to be used for reaching the best signal to background ratio. We will discuss the cut optimization issues in later sections of this note.

### 3 Electron and muon identification

For candidate events of the decays  $B_s^0 \rightarrow e^+\mu^-$  and  $B_d^0 \rightarrow e^+\mu^-$ , additional selections are performed on the track pairs to identify the tracks as electron or muon candidates.

The electron identification uses both the central calorimeter and the specific ionization  $dE/dx$  measured in the COT. The track-based electron-reconstruction algorithm [15] [16] [17] takes a good quality track with a minimal transverse momentum ( $p_T$ ) of 1 GeV/c and extrapolates it to the Central Strip chamber (CES) and the Central Preradiator (CPR). Along the projected trajectory, Central Electro Magnetic calorimeter (CEM) towers, CES clusters, CPR/CPR2 clusters are sorted and matched to the trajectory to form the electron objects. The CPR/CPR2 and CES clustering algorithms are described in references [18] [19] [20]. The matching to the CEM tower is done using  $\eta$  and  $\phi$  positions and a hit tower is required to have a minimal energy of  $50 \text{ MeV}/c^2$ . A 2-tower cluster is formed using the nearest tower in  $Z$  to the hit tower and the total electromagnetic (EM) energy and hadronic (HAD) energy are calculated from these two towers. For a track to be identified as electron, it must pass a set of calorimeter-based cuts using nine variables from the soft electron algorithm. The nine variables are described in detail in [17]. Table 4 lists the values of the

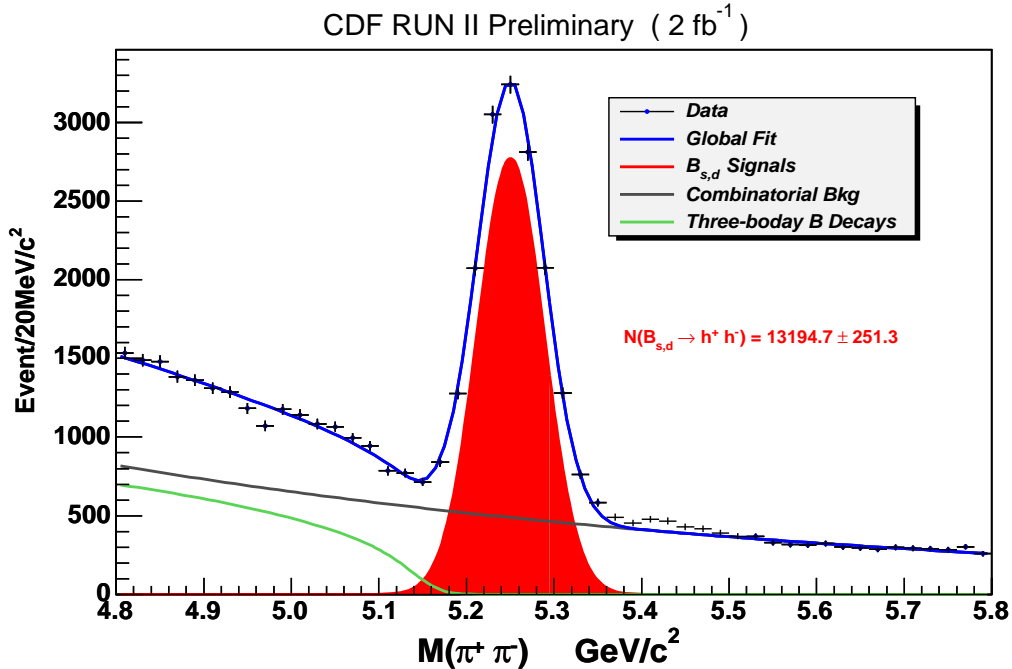


Figure 5:  $B \rightarrow h^+h^-$  invariant mass distribution after the common selection cuts have been applied. The data (dots with error bars) is superimposed with the fitted curve (blue line). The components of the fit function are: the  $B \rightarrow h^+h^-$  signal (red filled area) parameterized by a Gaussian function, the combinatorial background (black line) parameterized by an exponential function, and the physics background (green line) parameterized by a smeared Argus function.

cuts. We measure the selection efficiencies, shown in Table 5, using electrons selected from photon conversion samples. The photon conversion samples, *plbc0d*, *blpc0h*, *blpc0i* and *blpc0j* with the same run range as the TTT sample, 138809 - 241664, were collected with one electron track from  $\gamma \rightarrow e^+e^-$  decay in the the central electron trigger with  $p_T > 8\text{GeV}/c$ . The 2nd electron in the conversion is reconstructed using tracking info only and is used for electron efficiency measurement.

The specific ionization  $dE/dx$  as measured in the COT is a powerful variable to separate electron tracks from hadron tracks. The  $dE/dx$  calibration procedures are described in [21] and [22]. In addition to the calorimeter based variables described previously, the logarithm ratio between the measured  $dE/dx$  value and the expected value for electron tracks  $Z_e$  is used to identify electrons.

$$Z_e = \log[(dE/dx)_{\text{measurement}}/(dE/dx)_{\text{predict}}] \quad (4)$$

The pull variable defined as  $Z_e/\sigma_Z$  is used as the separation variable. We require candidates of electron tracks with  $Z_e/\sigma_Z > -1.3$  to keep most of the electrons while holding the hadron fake rate down. The choice of the cut is based on the dis-

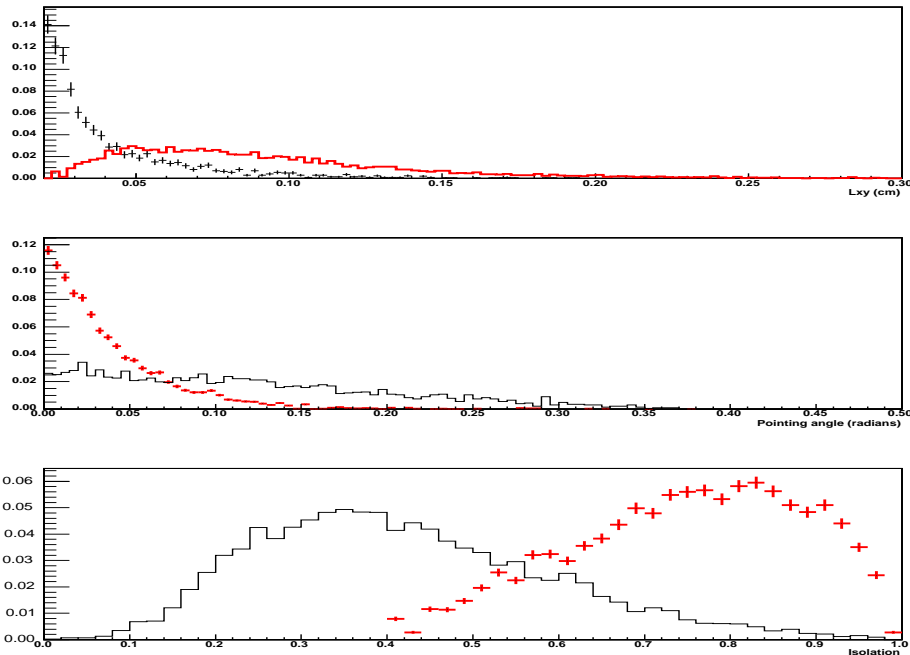


Figure 6: *Distribution of  $L_{xy}$ , pointing angle and Isolation for signal (red-colored points with error bars) and background (black-colored lines).*

Table 4: *Electron selection variables using calorimeters. The track of the electron candidate is required to point to the CES fiducial. In case the track passes through the fiducial region of CPR/CPR2 we also require a CPR/CPR2. CPR is used before run 190000 CPR2 is used for the later runs.*

Variable	cut
$E_{had}/E_{em}$	$had\_em\_Cal < 0.05$
$E/P$	$ep\_Cal > 0.7$
CES-Track match: $\Delta X$	$fabs(delta\_x\_CES) < 3.0$
CES-Track match: $\Delta Z$	$fabs(delta\_z\_CES) < 3.0$
Shower profile (wire readout)	$0 < chi2Wire < 20$
Shower profile (strip readout)	$0 < chi2Strip < 20$
$E_{CES}/p^*$	$eWire_{corr} > 0.02$
$E_{strip}/E_{wire}$	$swcorr\_Ces > 0.65$
CPR/CPR2 pulse height	$e\_cpr > 1.5$

tributions of this variable for electrons from photon conversion sample and various hadron samples [17], as shown in Figure 7. Again, we measure the selection efficien-

Table 5: *The electron identification efficiencies (%) of the calorimeter based algorithm and  $dE/dx$ . The values listed here are from the weighted averages from efficiencies measured in the three run periods of different  $dE/dx$  calibration status.*

$p_T$	2-3 GeV	3-4 GeV	4-5GeV	5-6GeV	> 6GeV
$\epsilon_{Cal}^{e^+}$	$0.6577 \pm 0.0049$	$0.7636 \pm 0.0044$	$0.8017 \pm 0.0049$	$0.8291 \pm 0.0054$	$0.8389 \pm 0.0039$
$\epsilon_{Cal}^{e^-}$	$0.6642 \pm 0.0049$	$0.7721 \pm 0.0046$	$0.8105 \pm 0.0051$	$0.8317 \pm 0.0057$	$0.8504 \pm 0.0040$
$\epsilon_{dE/dx}^{e^+}$	$0.938 \pm 0.021$	$0.936 \pm 0.024$	$0.933 \pm 0.030$	$0.927 \pm 0.044$	$0.906 \pm 0.031$
$\epsilon_{dE/dx}^{e^-}$	$0.936 \pm 0.020$	$0.934 \pm 0.026$	$0.926 \pm 0.037$	$0.917 \pm 0.046$	$0.903 \pm 0.038$

cies using  $dE/dx$ , shown in Table 5, using electrons selected from photon conversion samples. The efficiency was measured separately in three run periods, (A)138809-206898, (B)206990-228818 and (C)228810-241664. For data taken in periods (A) and (B), all 8 COT super layers were used for  $dE/dx$  measurements, while for data taken in period (C), the  $dE/dx$  readout from COT super layer 1 was disabled. Data taken in period (A) has run-dependent calibration constants available. For now we use the calibration constants obtained from the last few runs in period (A) for data taken in period (B) and (C) while waiting for the new calibration constants. We found the  $dE/dx$  efficiencies measured from the three period using the available constants vary by a few percent. For the preliminary result of the search in this note, we will use the weighted average of the three sets of efficiencies. The weights are calculated from the numbers of  $B \rightarrow h^+h^-$  events in each period. We assign a systematic uncertainty from the standard deviation of the three efficiencies sets, as listed in Table 5.

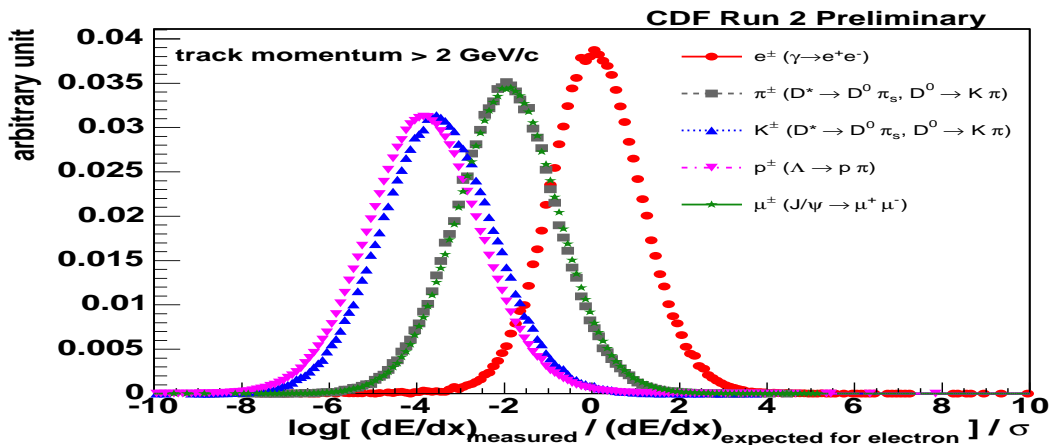


Figure 7: *Distributions of the  $Z_e$  pull charged tracks with  $p_T > 2 \text{ GeV}/c^2$ .*

The muon identification starts with the default “CdfMuon” collection [23]. We

only use CMU or CMX muons with a track-stub matching quality of  $\chi^2(\Delta r\phi) < 9$  between the positions measured using the muon chamber hits and that projected from the associated COT track. The minimum  $p_T$  requirement is 2.0 GeV for both CMU and CMX muons. The track-stub matching efficiencies are measured to be  $99.56 \pm 0.03\%$  [24] for CMU and  $99.13 \pm 0.05\%$  [25] for CMX, using muons from  $J/\psi$  decays. As stated before, we only use runs taken with good CMU and CMX detector conditions.

## 4 Measurement Optimization

The final step of the event reconstruction is the optimization of cuts to reach the best sensitivity for the  $B_{s,d}^0 \rightarrow e^+\mu^-$  searches. We chose to do the optimization varying three cuts: decay length  $L_{xy}$ , Isolation Iso and pointing angle  $\Delta\phi$  while keeping the other cuts fixed as in Table 3. Following the guidance outlined in [26], we will scan these three cuts to maximize the figure-of-merit ( $FOM$ ):

$$FOM = \frac{S}{\alpha/2 + \sqrt{B}} = \frac{S}{1.5 + \sqrt{B}} \quad (\text{with } \alpha = 3) \quad (5)$$

where  $S$  is the expected number of signal events and  $B$  is the expected background. (In the formula, the  $\alpha\sigma$  is the level of significance for a discovery. A popular choice is  $\alpha = 3$  for a  $3\sigma$  significance.)

The background distribution under the peak can be approximated using the events in the sideband of the peak. The background events to be used for the cut optimization are the reconstructed data events with an invariant mass in the windows of  $4.8 < M_{e\mu} < 5.0$  and  $5.72 < M_{e\mu} < 6.0$ , as shown in Figure 8. To increase the statistics, these background events are taken from the mass window without requiring a positive electron or muon identification.

To estimate the signal events, we use two methods. In the first method,  $S$  is estimated by fitting the invariant mass spectrum to obtain the number of  $B \rightarrow h^+h^-$  candidates. For this method, we assume the decays  $B_s^0 \rightarrow e^+\mu^-$  and  $B_d^0 \rightarrow e^+\mu^-$  have the same cut efficiency as for a typical  $B \rightarrow h^+h^-$  decay such as  $B_d^0 \rightarrow K^+\pi^-$ . We performed a simultaneous 3-dimensional scan for the three cuts. The projection of the scan are shown in Figure 9 and 10.

The second method of the cut optimization is to use the Monte Carlo events of  $B_s^0 \rightarrow e^+\mu^-$  to calculate  $S$ . Pure events of  $B_s^0$  without background are generated using “Bgenerator” and forced to decay 100% to  $B_s^0 \rightarrow e^+\mu^-$  using EvtGen, following the instructions outlined in [28]. We select events with  $p_T(B_s^0) > 2$  GeV and  $|\eta| < 1.3$  before sending them to full detector and trigger simulation. For SVT/XFT trigger simulations, we use a run-dependent beam-line for runs in the range of 138809 to 212133. We also correct the softer  $p_T$  spectrum from default setting in “Bgenerator” by re-weighting the reconstructed Monte Carlo using a function derived from comparing the  $B \rightarrow h^+h^-$  data  $p_T(B)$  to that of the  $B_d^0 \rightarrow K^+\pi^-$  Monte Carlo. The  $p_T$

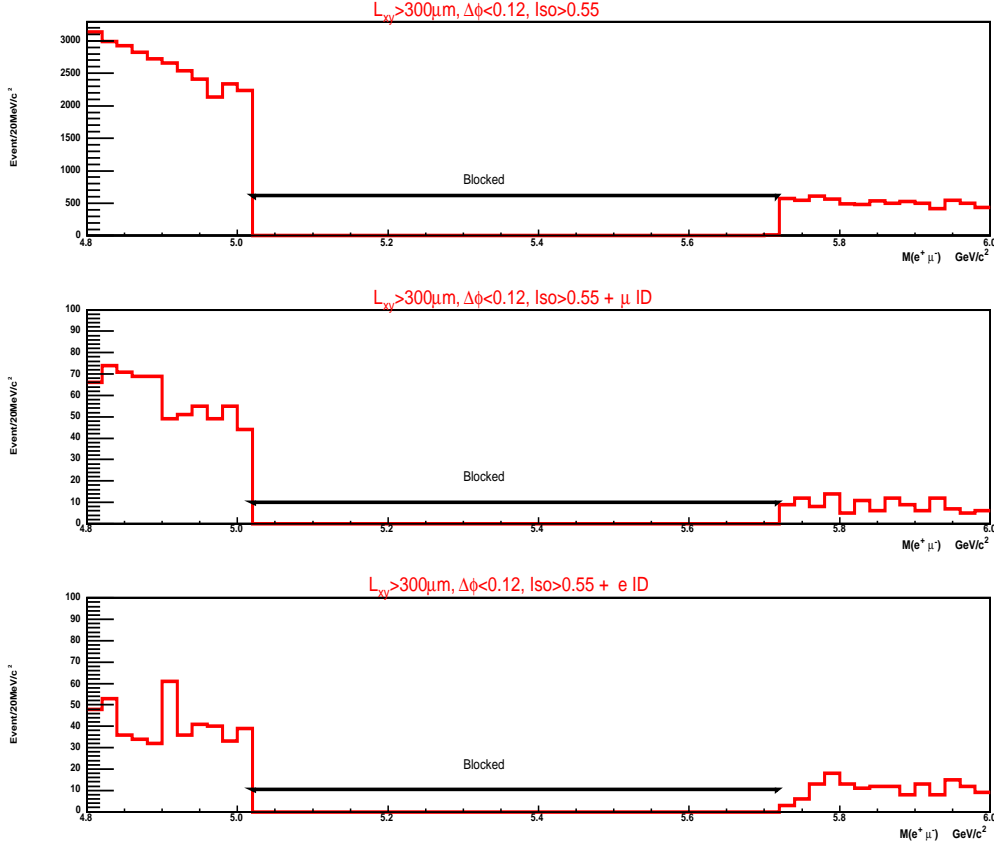
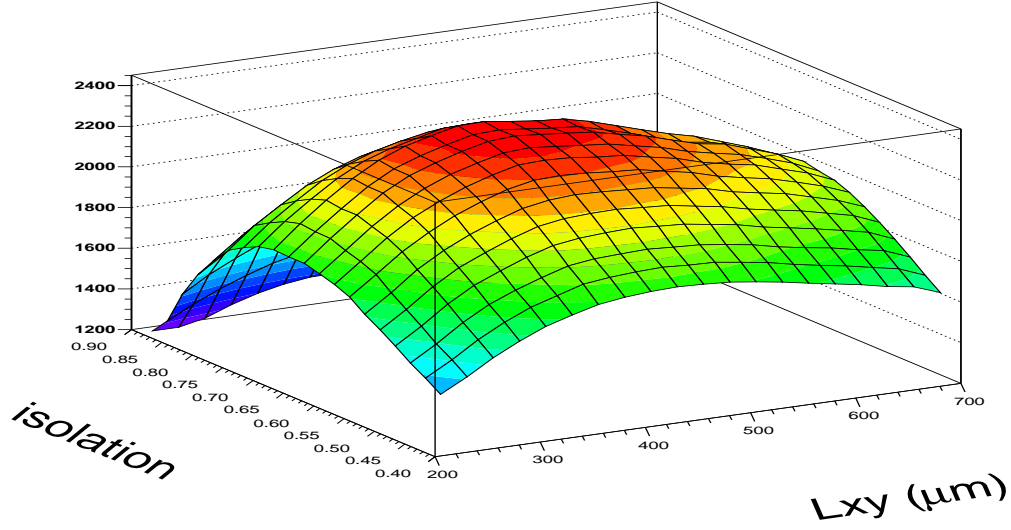


Figure 8: *Invariant mass distributions from two-body  $B$  decay candidates which passed the basic cut as in Table 3. The top plot is candidates with electron and muon assignments for the two daughter tracks without applying the electron and muon identifications. The middle plot is with one track identified as muon. The bottom plot is with one track identified as electron.*

spectra before and after weighting are shown in Figure 11 together with the weighting function. In Figure 12, we compare various distributions for data of  $B \rightarrow h^+h^-$  and Monte Carlo. Finally, the Monte Carlo events of  $B_s^0 \rightarrow e^+\mu^-$  were reconstructed in a similar way as the data and the scan of cuts is performed in the same fashion as before but using Monte Carlo events as input to calculate  $S$ . Again, a simultaneous 3-dimensional scan for the three cuts is performed and projections of the scan results are shown in Figure 13 and 14.

Both methods find that a cut combination of  $\Delta\phi < 0.11$ ,  $\text{Iso} > 0.675$  and  $L_{xy} > 375 \mu\text{m}$  gives good efficiency for the signal and good background rejection resulting in the highest  $FOM$  value. We choose these values for our final selection before lepton requirements are applied. Figure 15 shows the  $B \rightarrow h^+h^-$  invariant mass distribution after optimized cuts have been applied.

**lxy vs iso**



**lxy vs point**

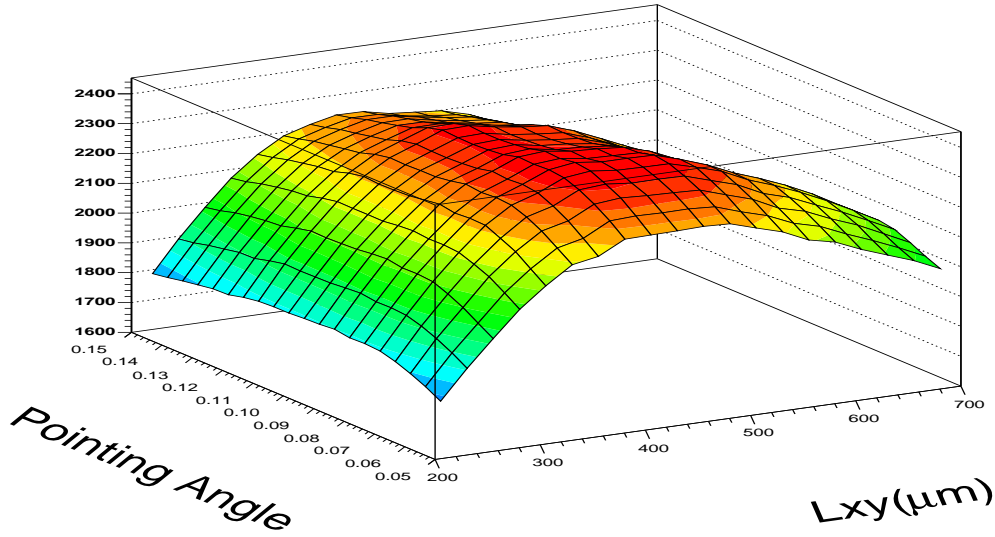


Figure 9: Cut scan using  $B \rightarrow h^+h^-$  candidates as an estimate for signal events and sideband events in the  $M_{e\mu}$  distribution as background events. The top plot shows a 2-d scan result of the Figure-of-Merit (FOM) as function of  $L_{xy}$  and Isolation. The bottom plot is the 2-d scan result of the FOM as function of  $L_{xy}$  and pointing angle.

iso vs point

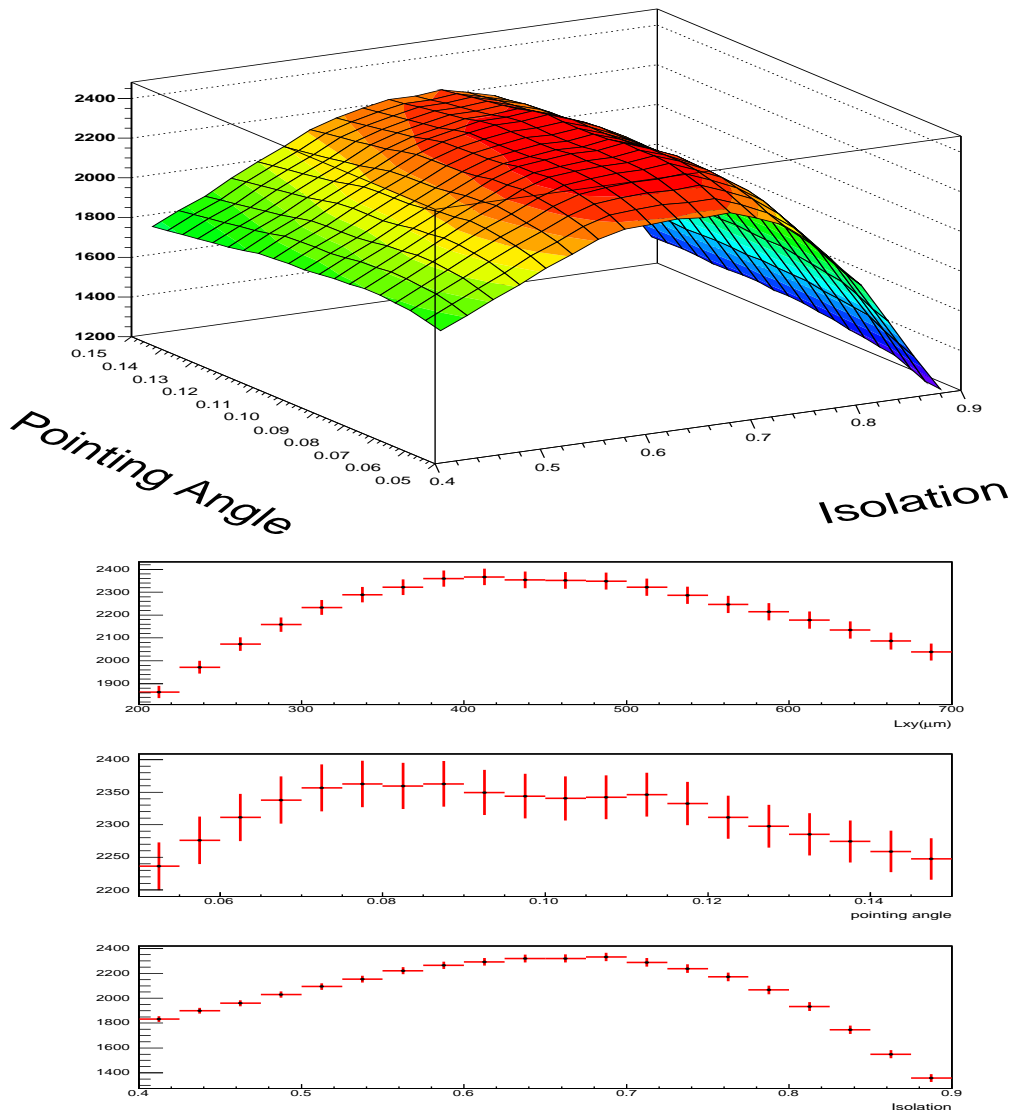


Figure 10: *Cut scan using  $B \rightarrow h^+h^-$  candidate events as an estimate for signal events and sideband events in the  $M_{e\mu}$  distribution as background events. The top plot is a 2-d scan result of the FOM as function of Isolation and pointing angle. The bottom plot is the projected scan of the FOM as function of  $L_{xy}$ , Isolation and pointing angle. For the projection of the FOM as function of one cut, the other two are fixed with values corresponding the best guess of the optimized values,  $Iso = 0.675$ ,  $\Delta\phi = 0.11$  and  $L_{xy} = 375 \mu\text{m}$ .*

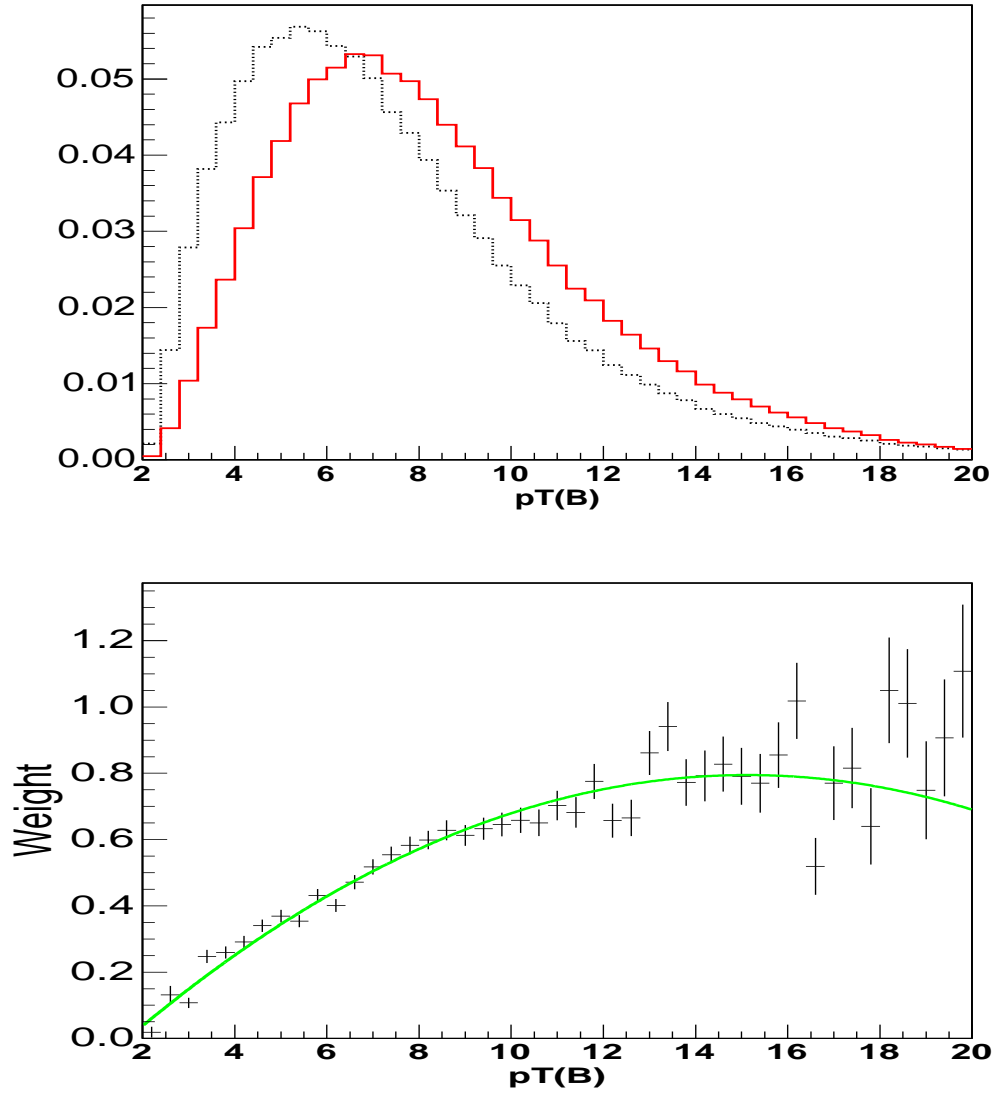


Figure 11: *Top: Monte Carlo  $p_T(B)$  spectrum before and after re-weighting. Bottom: Re-weighting function to correct the Monte Carlo  $p_T(B)$  spectrum.*

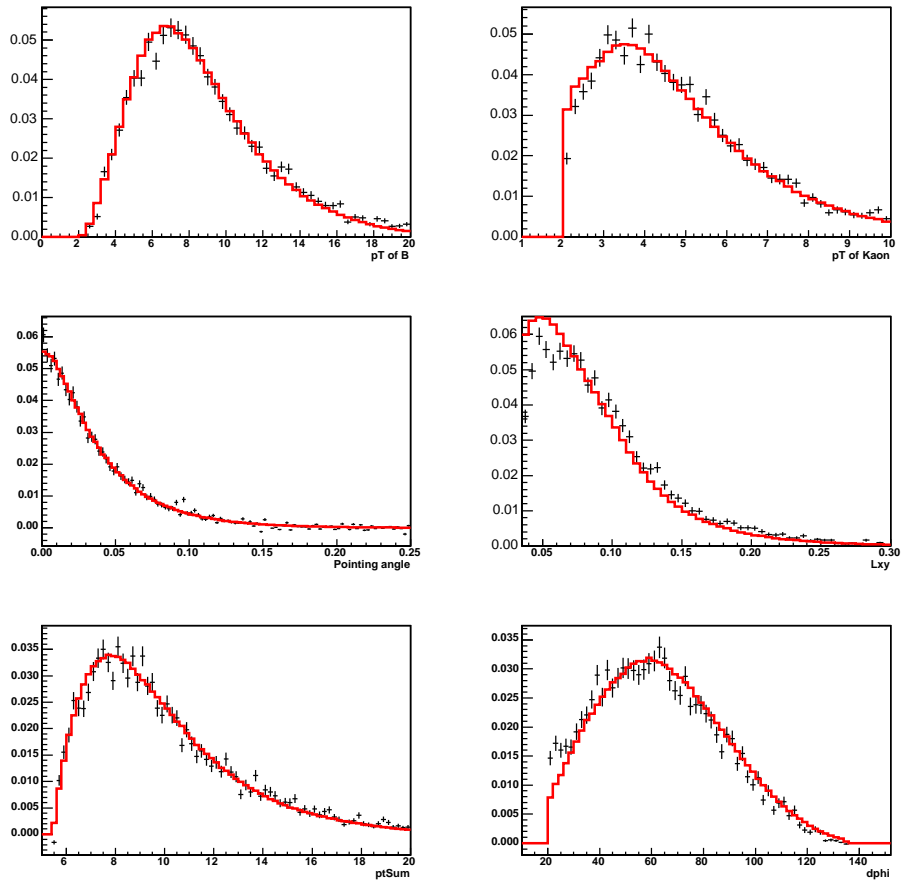
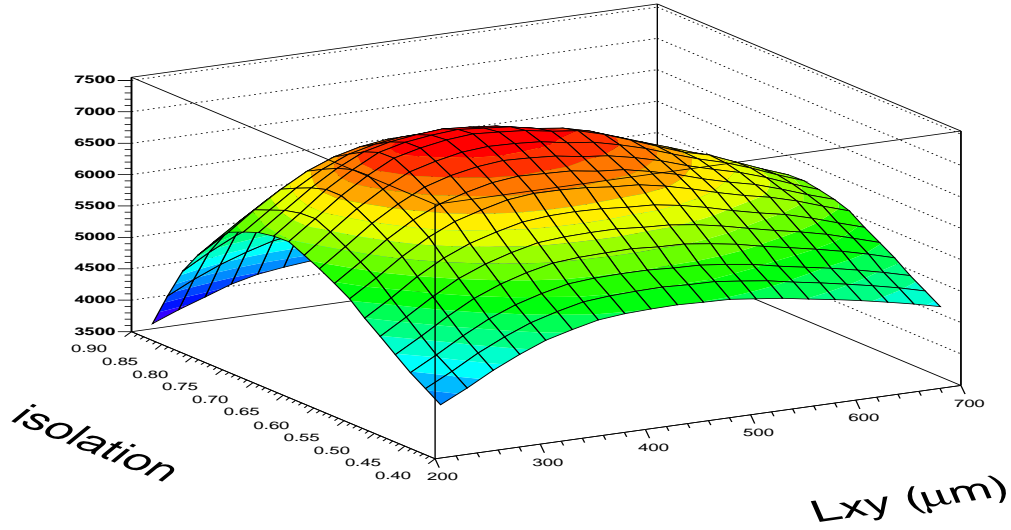


Figure 12: Comparison of data and Monte Carlo. Good agreement between the Monte Carlo and the data is achieved after re-weighting.

**lxy vs iso**



**lxy vs point**

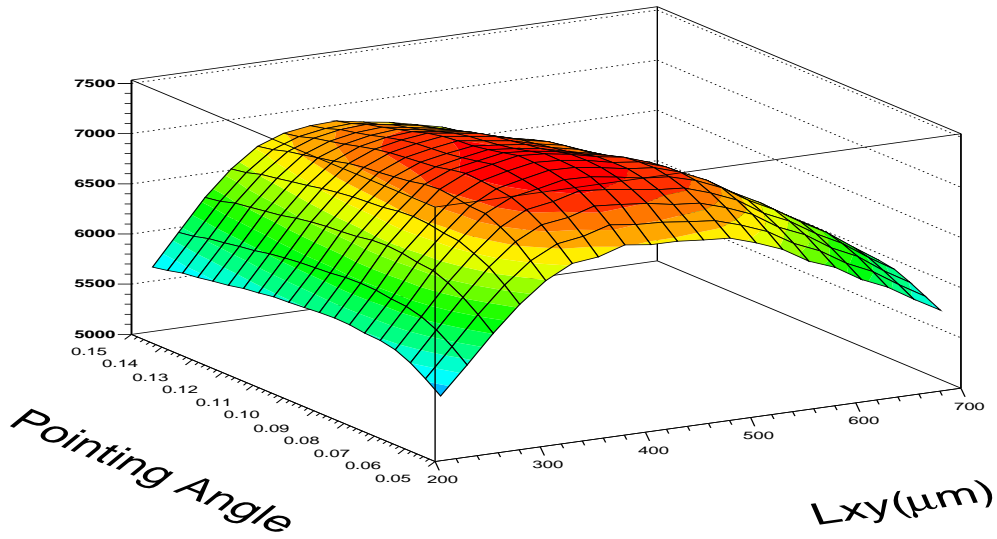


Figure 13: Cut scan using  $B_s^0 \rightarrow e^+\mu^-$  Monte Carlo events as estimate for signal events and sideband events in  $M_{e\mu}$  distribution as background events. The top plot shows the 2-d scan result for the Figure-of-Merit (FOM) as a function of  $L_{xy}$  and Isolation. The bottom plot shows the 2-d scan result of the FOM as function of  $L_{xy}$  and pointing angle.

**iso vs point**

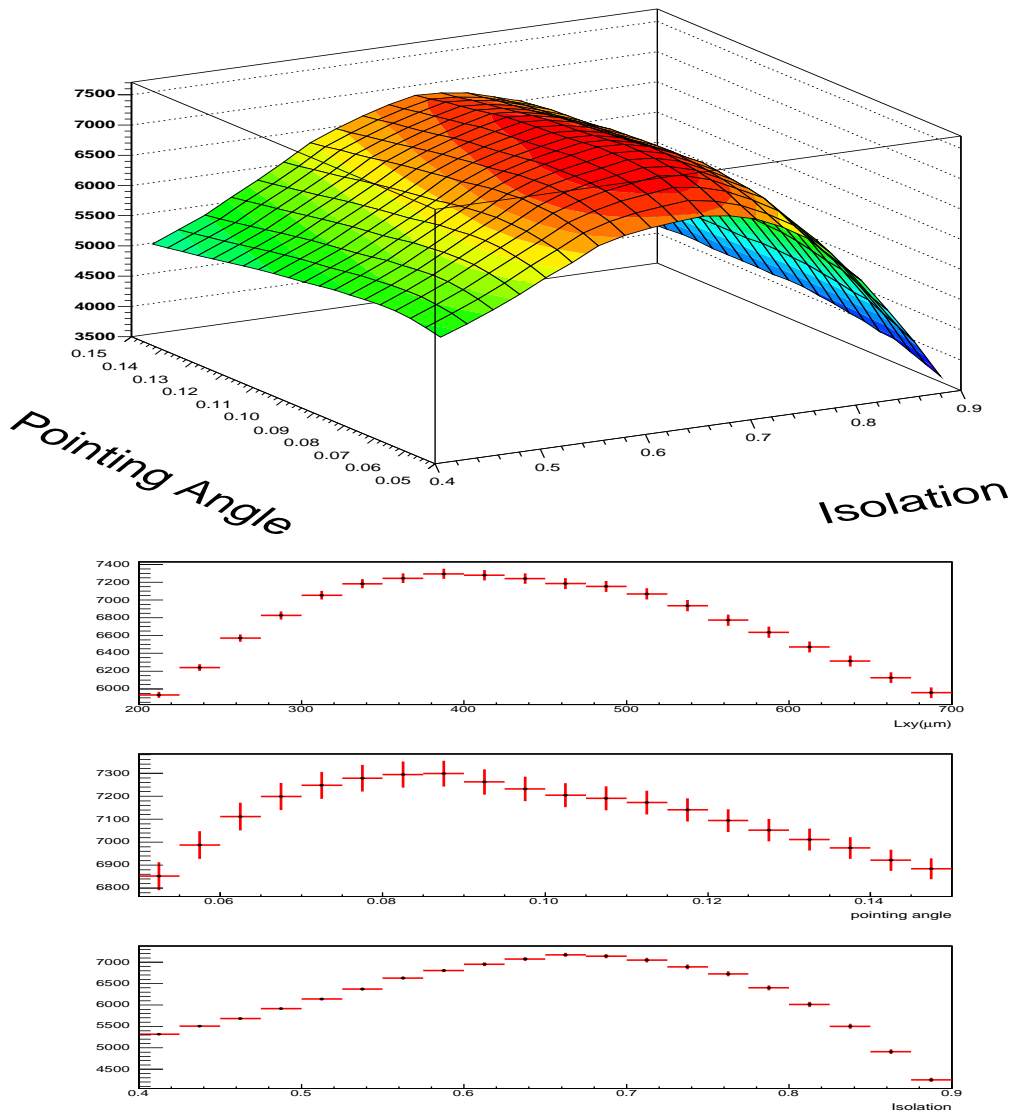


Figure 14: *Cut scan using  $B_s^0 \rightarrow e^+\mu^-$  Monte Carlo events as estimate for signal events and sideband events in  $M_{e\mu}$  distribution as background events. The top plot shows the 2-d scan result of the FOM as function of Isolation and pointing angle. The bottom plot shows the projected scan of the FOM as a function of  $L_{xy}$ , Isolation and pointing angle. For the projection of FOM as function of one cut, the other two are fixed with values corresponding the best guess of the optimized values,  $Iso = 0.675$ ,  $\Delta\phi = 0.11$  and  $L_{xy} = 375 \mu m$ .*

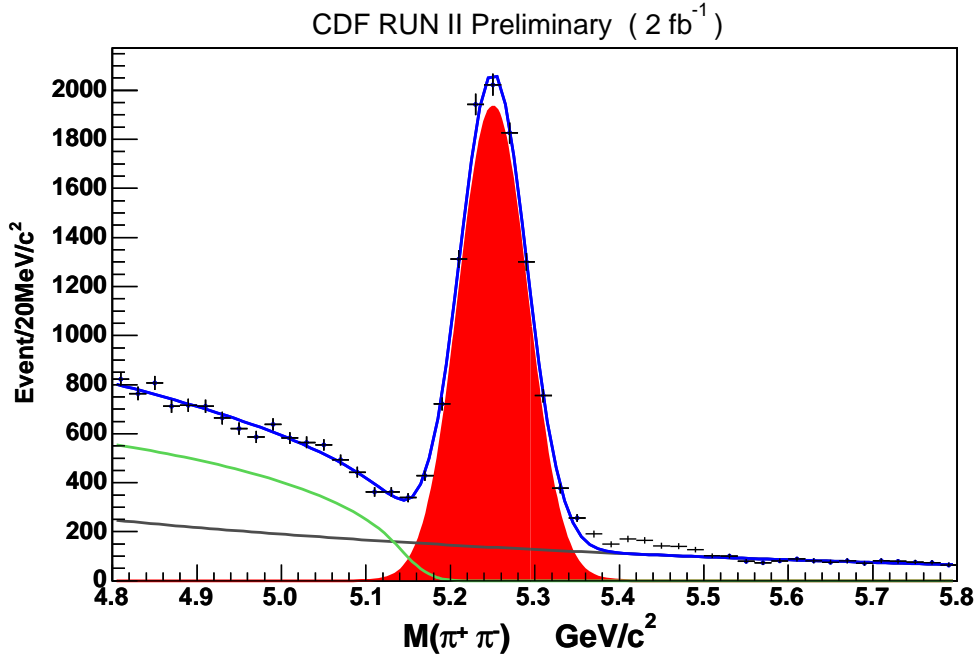


Figure 15:  $B \rightarrow h^+ h^-$  Invariant mass distribution with the optimized cuts of  $\Delta\phi < 0.11$ ,  $\text{Iso} > 0.675$  and  $L_{xy} > 375 \mu\text{m}$ . The result of the fit (blue line) is superimposed to the data (dots with error bars). The fitting function has three components: the  $B \rightarrow h^+ h^-$  signal (red filled area) parameterized as a Gaussian function, the combinatorial background (brown line) parameterized as an exponential, and the physics background (green line) parameterized as a smeared Argus function. The fit gives  $9648.4 \pm 224.7$  signal events of which we estimate that  $6387.0 \pm 214.4$  events are from the decay  $B_d^0 \rightarrow K^+ \pi^-$ .

## 5 Search Windows and Event Counting

We search for  $B_{s,d}^0 \rightarrow e^+\mu^-$  decay candidates in the mass window  $\pm 3\sigma$  around the  $B_{s,d}^0$  mass. To calculate the invariant mass the tracks of the electron/muon candidate are assigned the electron/muon mass respectively and the tracks are refitted with the correct  $DE/dx$  and multiple scattering estimates. We use the PDG values for the  $B$ -meson masses and the mass reconstruction resolution for two-body decays at CDF as obtained from fitting the  $B \rightarrow h^+h^-$  data, the search windows are (5.2616-5.4773)  $\text{GeV}/c^2$  for  $B_s^0 \rightarrow e^+\mu^-$  and (5.1713 - 5.3871)  $\text{GeV}/c^2$  for  $B_d^0 \rightarrow e^+\mu^-$ .

The signature of a signal event in the invariant mass distribution is a peak typically described by a Gaussian function. In the presence of energy loss due to electron Bremsstrahlung, the peak structure from  $B_s^0 \rightarrow e^+\mu^-$  and  $B_d^0 \rightarrow e^+\mu^-$  decays will be distorted by a long tail below the  $B_{s,d}^0$  nominal mass, as shown in Figure 16 from a Monte Carlo simulation. This tails lead to a lower efficiency of the mass window cuts with respect to the  $B \rightarrow h^+h^-$  and so contributes to the lower efficiency and acceptance of the decays  $B \rightarrow e^+\mu^-$  relative to that of the decay  $B_d^0 \rightarrow K^+\pi^-$ .

Figure 17 shows the invariant mass distributions for  $e\mu$  pairs after all cuts have been applied. We observe one event in the  $B_s^0$  mass window and two events in the  $B_d^0$  mass window. These numbers are consistent with the number of events observed in the region outside the mass window. We estimated background contributions of  $0.81 \pm 0.63$  events in the  $B_s^0$  mass window and  $0.94 \pm 0.63$  in the  $B_d^0$  mass window from combinatorial and double lepton-fakes from  $B \rightarrow h^+h^-$ .

The combinatorial background can come from sources such as multi-body  $B$  decays such as sequential semileptonic decays, gluon splittings where electron and muon are decay products from different  $B$  or charm mesons,  $B\bar{B}$  decays where the electron and muon are from different  $B$ 's, and purely random combinations from either real leptons or fake leptons. We assume the size of the contributions can be estimated by counting events outside the signal mass window and normalizing this number to the size of the signal mass windows. We have two events in the low sideband and zero events in the high sideband, as shown in Figure 17. We estimate the number of combinatorial events per 1 GeV window as:  $(2+0)/(2*0.2994) = 3.34$  events/GeV with statistic error of 2.34 event/GeV and systematic error 1.76 events/GeV. The statistic error is taken from the the square root of event numbers and the systematic error is estimated by varying the size and positions of the sideband windows. The biggest change is from re-positioning the sideband windows to include all events outside the  $3\sigma$  search window around  $B_{s,d}^0$  nominal mass. Projecting this into the search signal mass window, we estimate  $(3.34 \pm 2.93) \times 0.2158 = 0.72 \pm 0.63$  combinatorial background events for the  $B_s^0 \rightarrow e^+\mu^-$  and  $B_d^0 \rightarrow e^+\mu^-$  channels.

To estimate the double  $e\mu$  fake rate from  $B \rightarrow h^+h^-$ , we first obtain the  $p_T$ -dependent kaon and pion electron and muon fake rate measured with similar electron and muon selection criteria in [17] and [29]. For electrons, Tables.4 and Table.30 in [17] are used for  $dE/dx$  and calorimeter-based selection. For muons, Tables 5 and 6

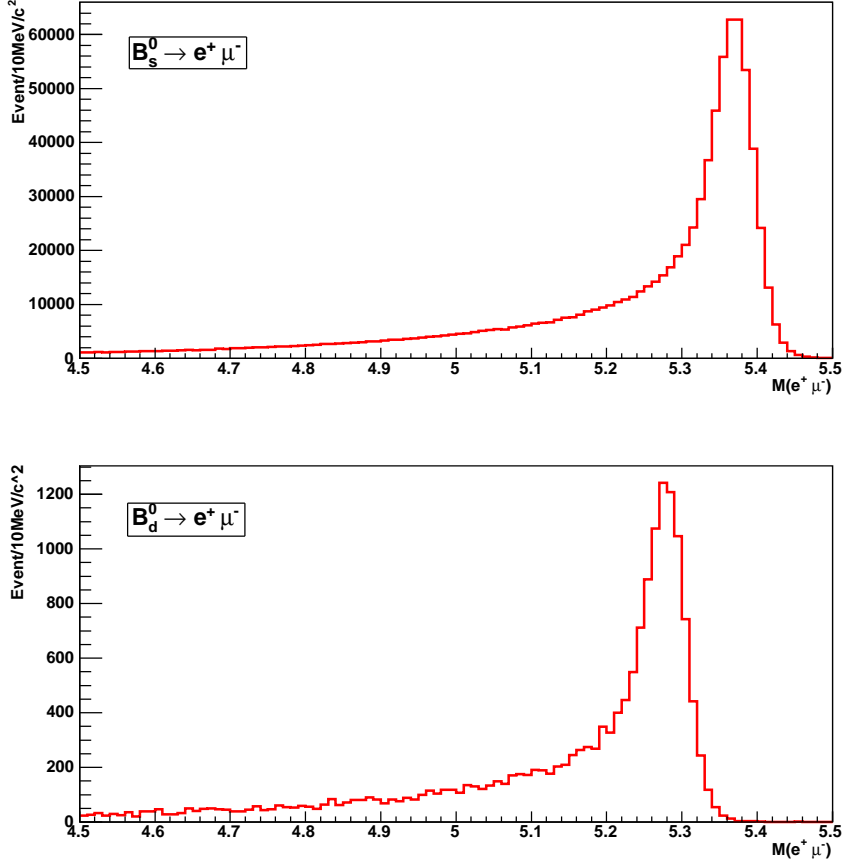


Figure 16: Monte Carlo invariant mass distributions for  $B_s^0 \rightarrow e^+ \mu^-$  and  $B_d^0 \rightarrow e^+ \mu^-$ .

are used for SVT pion and Kaon tracks. To get the averaged Kaon/pion fake electron and muon rates, raw yield results of  $B_{s,d} \rightarrow K\pi, KK, \pi\pi$  in Table 8 of [14] are used to obtain the fractions of pion and Kaon tracks in the  $B \rightarrow h^+ h^-$  events. The averaged hadron track fake electron and muon rates are thus calculated using the Kaon and pion track fractions together with their fake probabilities.

- To check the fake rate calculation, we weight the  $B \rightarrow h^+ h^-$  events with the  $p_T$ -dependent electron or muon rates for a prediction of the single electron or muon contributions. The predicted single fake events are compared to the events of  $B \rightarrow h^+ h^-$  with one leg identified by the electron or muon packages. The results are shown in Figure 18. The predicted single fake events,  $37.6 \pm 5.6$  for electrons and  $112 \pm 16.8$  for muons, agree well with single electron/muon identified  $B \rightarrow h^+ h^-$  events,  $47.3 \pm 10.4$  for electron and  $121.1 \pm 14.3$  for muon.
- The double electron-muon fake events are estimated by applying the electron and muon fake rate to the two tracks in  $B \rightarrow h^+ h^-$ . We obtain an estimate of

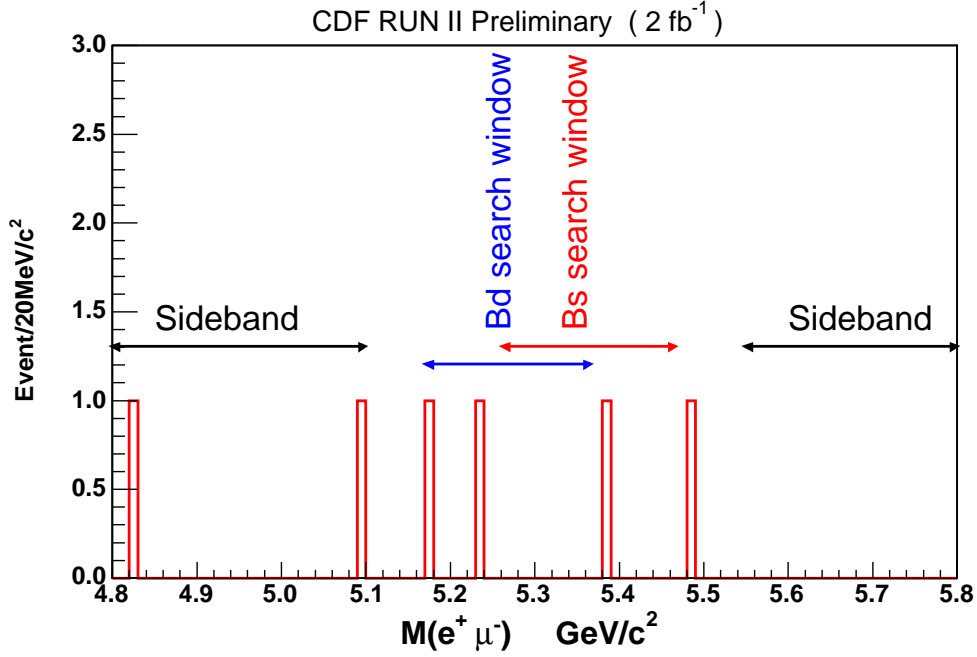


Figure 17: Invariant mass distributions of the electron and muon track pairs for events that passed both electron and muon identification.

$0.229 \pm 0.046$ , as shown in Figure 19. Due to the wrong mass assignment, the fractions of  $B \rightarrow h^+h^-$  events with  $e - \mu$  mass assignments in our  $B_{s,d}^0 \rightarrow e^+\mu^-$  search windows are  $0.39 \pm 0.01$  ( $B_s^0$ ) and  $0.98 \pm 0.01$  ( $B_d^0$ ). Finally, the double  $e - \mu$  fake contributions are estimated to be  $0.09 \pm 0.02$  for  $B_s^0$  and  $0.22 \pm 0.04$  for  $B_d^0$ .

To summarize this section, we observe one event in the  $B_s^0 \rightarrow e^+\mu^-$  mass window with estimated  $0.81 \pm 0.63$  background events and two events in the  $B_d^0 \rightarrow e^+\mu^-$  mass window with estimated  $0.94 \pm 0.63$  background events. The number of events we observe are consistent with the estimated background contributions.

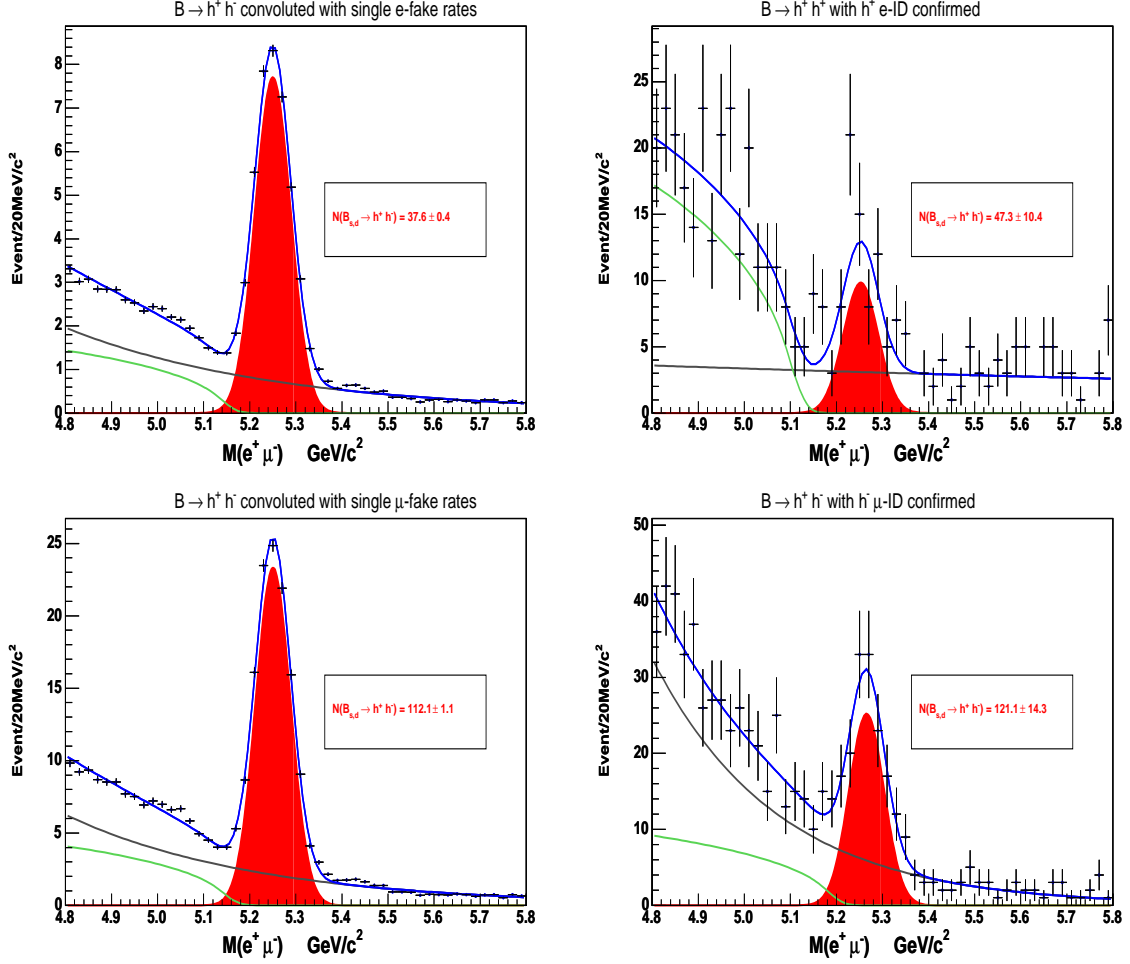


Figure 18: Invariant mass distribution of  $B_{s,d}^0 \rightarrow h^+ h^-$  events with electron and muon mass assignments for the two tracks. Top plots are for events weighted with single electron fake rate (left) or one track identified as electron (right). The bottom plots are for events weighted with single muon fake rate (left) or one track identified as muon (right).

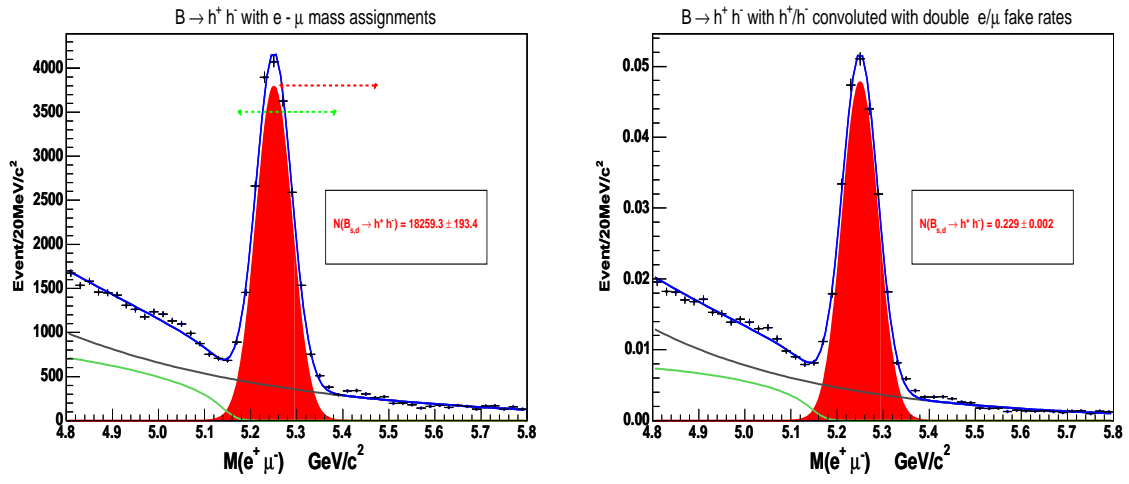


Figure 19: Invariant mass distribution of  $B_{s,d}^0 \rightarrow h^+ h^-$  events with electron and muon mass assignments for the two tracks. The right plot is from events weighted by double  $e - \mu$  fake rates.

## 6 Relative Efficiency and Acceptance

In order to calculate the branching ratio from the observed event candidates, we need to know the reconstruction efficiency. The efficiency calculations for  $B_s^0 \rightarrow e^+\mu^-$  and  $B_d^0 \rightarrow e^+\mu^-$  are very similar so we will only describe  $B_s^0 \rightarrow e^+\mu^-$  in detail. As stated previously in Equation 2, we choose to calculate the efficiency for  $B_s^0 \rightarrow e^+\mu^-$  relative to that of the decay  $B_d^0 \rightarrow K^+\pi^-$ ,  $\epsilon_{B_s^0 \rightarrow e^+\mu^-}^{rel}$ . This way, many of the common reconstruction efficiencies due to tracking, triggering, and vertexing, cancel. The remaining effects that still have to be considered are the relative detector and kinematic acceptance  $A_{rel}$  including the mass window requirement and the electron and muon identification efficiencies.

- We use Monte Carlo events of  $B_s^0 \rightarrow e^+\mu^-$  and  $B_d^0 \rightarrow K^+\pi^-$  to estimate the detector and kinematic acceptance. These events are generated in the same fashion as those used to do the cut optimization as described in section 4. All tracks in the three decays are required to pass the same set of cuts as in Table 3. In addition, the events from  $B_s^0 \rightarrow e^+\mu^-$  are required to be in the mass window of (5.2616 - 5.4773) GeV/ $c^2$ . No specific electron and muon identifications are required for Monte Carlo tracks except the tracks are required to be within pseudo-rapidity of 1.
- For the fiducial coverage of electron and muon, we use the coverage efficiencies obtained from measurements using data. The CEM/CES fiducial coverage is measured to be  $80.0 \pm 0.78\%$  using tracks from  $J/\psi \rightarrow \mu^+\mu^-$  [17]. The CMU and CMX muon fiducial coverage are also from measurements [29] using data, as  $70.35 \pm 0.64\%$  for CMU and  $39.35 \pm 1.01\%$  for the CMX. The CES/CPR and dE/dx cut efficiencies, as measured using conversion electrons, are listed in Table 5. The track-stub matching efficiency is  $99.56 \pm 0.03\%$  [24] for CMU and  $99.13 \pm 0.05\%$  [25] for CMX.

Monte Carlo events within the detector and kinematic acceptance are re-weighted using weights calculated from electron and muon fiducial coverage and identification efficiencies on an event-by-event base to take into considerations of kinematic dependences of these efficiencies for  $B_s^0 \rightarrow e^+\mu^-$  and  $B_d^0 \rightarrow K^+\pi^-$ . The final ratio of efficiency and acceptance for  $B_s^0 \rightarrow e^+\mu^-$  and  $B_d^0 \rightarrow K^+\pi^-$  is thus the ratio of the event counting with the re-weighting. We obtain

$$\epsilon_{B_s^0 \rightarrow e^+\mu^-}^{rel} = 0.2071 \pm 0.0003 \pm 0.0158$$

$$\epsilon_{B_d^0 \rightarrow e^+\mu^-}^{rel} = 0.2097 \pm 0.0023 \pm 0.0123$$

where the first error is the statistical and second is the systematic error.

The source of the systematic errors considered and the magnitudes are listed in Table 6. To estimate the systematic error on the relative efficiency, we vary the values

for CMU/CMX/CEM/ fiducial coverage, CMU/CMX track-stub matching efficiencies, dE/dx cut efficiencies and CES/CPR cut efficiencies according to the measurement errors by  $\pm$  one standard deviation and regard the changes on the total relative efficiency as the error. For  $B_s^0 \rightarrow e^+\mu^-$  events, about 39% of the events fall outside the search window and into the long tail due to the energy loss from electron Bremsstrahlung as shown in Figure 16. The estimation of the efficiency loss due to electron Bremsstrahlung depends on the precise accounting of detector materials in the Monte Carlo simulation. We assume the amount of material is accurate to about 10% for beam-pipe, silicon detector and COT. We estimate the effect caused by material on the relative efficiency assuming by applying a 10% error to the number of events outside the search window in Figure 16. We assign a 3.9% systematic error on the relative efficiency due to the precision of the accounting of detector material. The systematic error from  $p_T$  threshold come from the biggest changes of the relative efficiencies ( $\Delta\epsilon^{rel} = 0.05$ ) for events with  $p_T(e) + p_T(\mu) < 6.0 \text{ GeV}/c^2$ , shown in Figure 20, together with fraction (3%) of events in this  $p_T$  region. To estimate the systematic error due to uncertainties related with the  $p_T(B_s)$  spectrum, we compare results obtained by using the two spectra as shown in Figure 11. To estimate the uncertainty from the  $B_s^0$  lifetime, we use an alternative Monte Carlo sample with  $B_s$  lifetime taken the PDG value of that for  $B_d^0$ . The lifetime difference between the one used in default Monte Carlo sample (PDG for  $B_s$  lifetime) and the alternative samples are about three times bigger than the error on the  $B_s$  lifetime itself. We found the change on the efficiency ratio is about 3%.

Source	Change [%]
CMU fiducial	0.74
CMU Matching	0.024
CMX fiducial	0.63
CMX Matching	0.01
dE/dx	3.3
CEM fiducial	0.97
CES/CPR Cuts	2.1
Detector Material	3.9
$p_T$ threshold	1
$p_T(B_s)$ Spectrum	4
$c\tau(B_s)$	3
$\epsilon_{Rel}$ Total	7.62

Table 6: *Systematic uncertainties affecting  $\epsilon_{Rel}$  for  $B_s^0 \rightarrow e^+\mu^-$ . The systematic uncertainties affecting  $B_d^0 \rightarrow e^+\mu^-$  are similar to that of  $B_s^0 \rightarrow e^+\mu^-$  except no systematic error is assigned from lifetime for  $B_d^0 \rightarrow e^+\mu^-$ .*

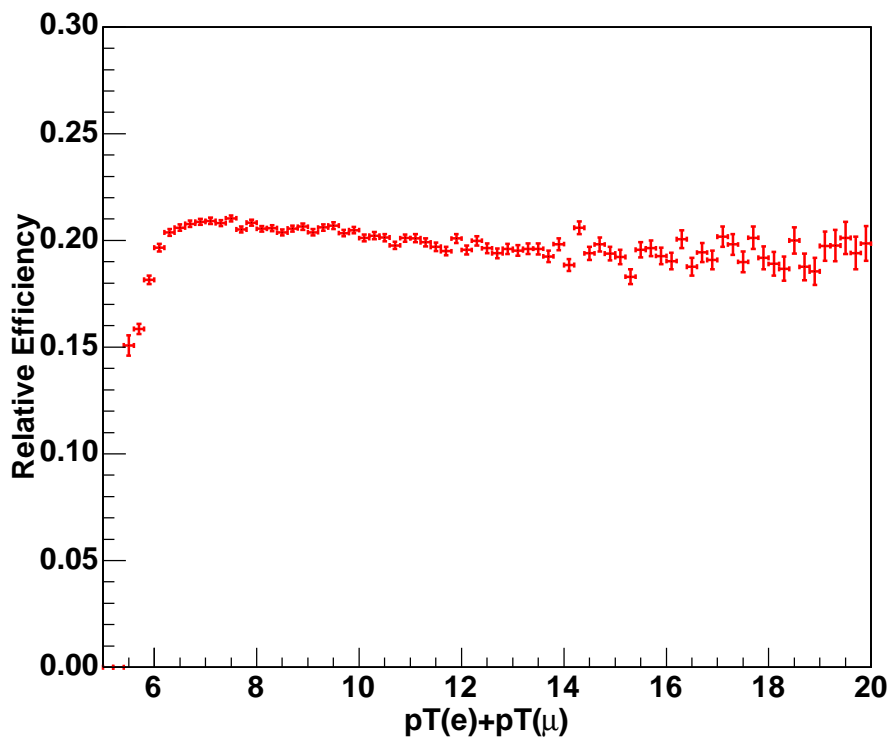


Figure 20: *Relative efficiency as a function of  $p_T(e) + p_T(\mu)$ .*

## 7 Limits on the branching ratios and Leptoquark masses

As shown in Equations 3 and 2, the ingredients we need to calculate the branching ratio limits are: the number of signal  $B_{s,d}^0 \rightarrow e^+\mu^-$  events (or limit thereof)  $N(B_{s,d}^0 \rightarrow e^+\mu^-)$ , the number of reconstructed events of the reference channel  $N(B_d^0 \rightarrow K^+\pi^-)$  and its branching ratio  $Br(B_d^0 \rightarrow K^+\pi^-)$ , the relative detector and selection efficiency  $\epsilon_{B_{s,d}^0 \rightarrow e^+\mu^-}^{rel}$ , and for  $B_s^0$  only the relative production rates of  $B_s^0$  versus  $B_d^0$ ,  $f_{B_s^0}/f_{B_d^0}$ . The number of events of  $B_d^0 \rightarrow K^+\pi^-$  is obtained by fitting the  $M_{\pi\pi}$  mass distribution, as shown in Figure 15, and by using the sample composition result [14] in the sample obtained in a very similar environment. We obtain  $6387.0 \pm 214.4$  events of  $B_d^0 \rightarrow K^+\pi^-$  in the sample. The error here is a combination of the mass fitting error (2.3%) and also the sample composition error (2.4%) including extra uncertainty (1.4%) related with different selection cuts used in this analysis and those used in the analysis of reference [14]. The uncertainty on the measured sample composition from difference selection cuts was estimated by Michael Morello using fully reconstructed Monte Carlo events and varying the following cuts:  $L_{xy} > 300 \rightarrow 400\mu m$ ,  $d_0(1,2) > 100 \rightarrow 200\mu m$  on the two tracks and  $d_0(B) < 80 \rightarrow 40\mu m$ . The change on the measured sample composition is found to be in the order of 1.4%.

The decay branching ratio  $Br(B_d^0 \rightarrow K^+\pi^-) = 19.4 \pm 0.6 \times 10^{-6}$  [11] is the world average calculated by the Heavy Flavor Average Group (HFAG). The value of  $f_{B_d^0}/f_{B_s^0}$  obtained using world average of  $b$ -quark fragmentation fractions is  $(0.398 \pm 0.012)/(0.103 \pm 0.014) = 3.86 \pm 0.59$ , where the (anti-)correlation between the uncertainties has been accounted for [12]. The relative detector and selection efficiencies were obtained as  $\epsilon_{B_s^0 \rightarrow e^+\mu^-}^{rel} = 0.2071 \pm 0.0158$  and  $\epsilon_{B_d^0 \rightarrow e^+\mu^-}^{rel} = 0.2097 \pm 0.0123$ . In Table 7, we summarize the systematic uncertainties affecting the branching ratio calculation. We will assign a total uncertainty of 17.7% on the  $B_s^0 \rightarrow e^+\mu^-$  decay branching ratio calculation and 7.5% on  $B_d^0 \rightarrow e^+\mu^-$ .

Source	values	$\Delta Br(B_s^0 \rightarrow e^+\mu^-)$	$\Delta Br(B_d^0 \rightarrow e^+\mu^-)$
$N(B^0 \rightarrow K^+\pi^-)$	$6387.0 \pm 214.4$	3.4%	3.4%
$BR(B^0 \rightarrow K\pi)$	$(19.4 \pm 0.6) \times 10^{-6}$	3.1%	3.1%
$f_{B_d^0}/f_{B_s^0}$	$3.86 \pm 0.59$	15.3%	-
$\epsilon_{B_s^0 \rightarrow e^+\mu^-}^{rel}$	$0.2071 \pm 0.0158$	7.6%	-
$\epsilon_{B_d^0 \rightarrow e^+\mu^-}^{rel}$	$0.2097 \pm 0.0123$	-	5.9%
Total		17.7%	7.5%

Table 7: *Systematic uncertainties on the limits of  $Br(B_{s,d}^0 \rightarrow e^+\mu^-)$ .*

Now we can calculate the upper limit on the signal events of  $B_{s,d}^0 \rightarrow e^+\mu^-$  decays from the observed candidates and estimated background. We combine the systematic

uncertainties with the Poisson limits and perform background subtraction. To obtain the limits we employ two programs and compare the results. The first program is *POILIM* which uses the convoluted-likelihood function method [30]. The second program is *BAYES* which calculates upper limits using a Bayesian method with flat prior probability. For the final limits we will use the results obtained with *BAYES* which is recommended by the CDF statistics committee. The results are listed in Table 8. Limits obtained by the two programs are in good agreement. The table also lists the results without considering systematic uncertainties and with no background subtraction. In this case one expects the programs to reproduce the Poisson upper limits which for one observed event are 3.89(4.74) events at 90(95) % C.L. and for two observed events are 5.32(6.30) events at 90(95) % C.L.. We see that both programs reproduce the result for this special case. For the run I measurement we decided to be conservative and did no background subtraction therefore the results for this case are also listed to show the effect of background subtraction on the limit.

Search Channel	$N_{obs}$	$N_{bgr}$	Systematic uncertainty (%)	(BAYES)		(POILIM)	
				$N_{C.L.}^{90\%}$	$N_{C.L.}^{95\%}$	$N_{C.L.}^{90\%}$	$N_{C.L.}^{95\%}$
no systematics, no background subtraction							
$B_s$	1	0±0	0	3.89	4.74	3.89	4.74
$B_d$	2	0±0	0	5.32	6.30	5.32	6.30
systematics only							
$B_s$	1	0±0	17.7	4.21	5.20	4.08	5.05
$B_d$	2	0±0	7.5	5.40	6.41	5.37	6.37
systematics and background subtraction							
$B_s$	1	0.81±0.63	17.7	3.60	4.57	3.55	4.5
$B_d$	2	0.94±0.63	7.5	4.44	5.44	4.59	5.58

Table 8: *Upper limits on signal events of  $B_{s,d}^0 \rightarrow e^+ \mu^-$  from observed and estimated background events. Two programs (BAYES) and (POILIM) are compared and three background and systematic error conditions are shown. The systematic uncertainties are the summary of those affecting branching ratio calculations.*

Inserting the upper limit of signal events from  $B_{s,d}^0 \rightarrow e^+ \mu^-$  in the formulas 3 and 2. We obtain the following branching ratio limits:  $Br(B_s^0 \rightarrow e^+ \mu^-) < 2.0(2.6) \times 10^{-7}$  and  $Br(B_d^0 \rightarrow e^+ \mu^-) < 6.4(7.9) \times 10^{-8}$  at 90 (95) % confidence level. From these we derive limits on the masses of the corresponding Pati-Salam leptoquarks of  $M_{LQ}(B_s^0) > 47.7(44.6)$  TeV/c<sup>2</sup> and  $M_{LQ}(B_d^0) > 58.6(55.7)$  TeV/c<sup>2</sup> at 90 (95) % confidence level. The limits are also shown in Figures 21 and 22.

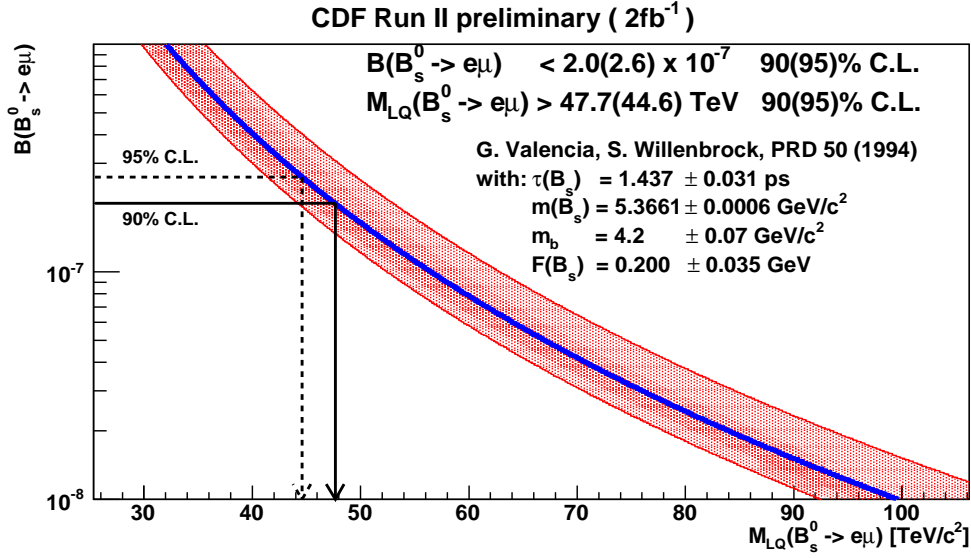


Figure 21: *Leptoquark mass limit corresponding to the 90 % C.L. on  $Br(B_s^0 \rightarrow e^+ \mu^-)$ .*

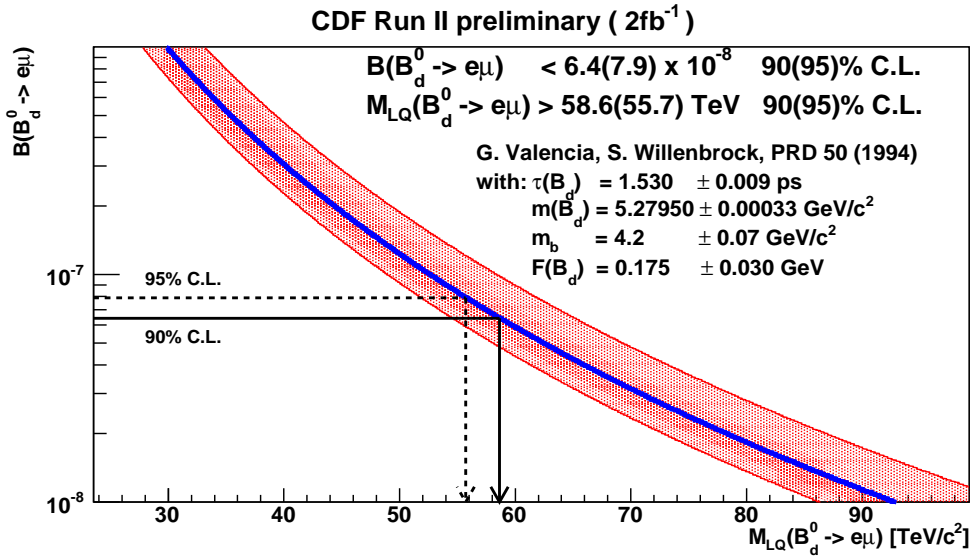


Figure 22: *Leptoquark mass limit corresponding to the 90 % C.L. on  $Br(B_d^0 \rightarrow e^+ \mu^-)$ .*

## 8 Search for the decays $B_{s,d}^0 \rightarrow e^+e^-$

Using the same data sample described in Section 2, we also carried out a search for the flavor changing neutral current decays  $B_{s,d}^0 \rightarrow e^+e^-$ . The event selections are kept the same as described in Table 3 with optimized values for isolation, pointing angle and decay length as  $Iso = 0.675$ ,  $\Delta\phi = 0.11$  and  $L_{xy} = 375 \mu m$ . The only difference is that now both tracks are required to have a minimum  $p_T$  of 2 GeV/ $c^2$  and have to be identified as an electron candidate using both  $dE/dx$  and calorimeter-based variables.

The signature of the  $B_{s,d}^0 \rightarrow e^+e^-$  is again a peak in the invariant mass distribution with the two tracks with electron mass assignment. Since both tracks in the decay now suffer the energy loss due to electron Bremsstrahlung in the detector, the tail below  $B_{s,d}^0$  mass is more pronounced, as shown in Figure 23 from a Monte Carlo simulation. To make up the loss of the efficiency due to the Bremsstrahlung effect, we will use an asymmetric search window,  $(-6\sigma, 3\sigma)$ , around the nominal value of the  $B_{s,d}^0$  masses. Using the resolution measured from the two-body B decay events, we define the search windows as  $(5.1542, 5.4773)$  GeV/ $c^2$  for the  $B_s^0 \rightarrow e^+e^-$  decay and  $(5.064 - 5.3871)$  GeV/ $c^2$  for the  $B_d^0 \rightarrow e^+e^-$  decay.

Figure 25 shows the invariant mass distributions for  $e^+e^-$  pairs after all cuts have been applied. We observe one event in the  $B_s^0$  mass window and two events in the  $B_d^0$  mass window. These numbers are consistent with the number of events observed in the region outside the mass window. We estimate background contributions of  $2.7 \pm 1.8$  events in either the  $B_s^0$  or  $B_d^0$  mass windows from combinatorial and double lepton-fakes from  $B \rightarrow h^+h^-$ . The combinatorial background is from counting events in the two sideband regions in the mass window as shown in Figure 23. We estimate  $2.66 \pm 1.19 \pm 1.35$  events projecting to the  $B_s^0$  and  $B_d^0$  search windows. The double electron fake rates from  $B \rightarrow h^+h^-$  are again estimated by re-weighting the  $B \rightarrow h^+h^-$  events with the  $p_T$ -dependent  $\pi/K$  hadron fake electron rates, as shown in Figure 24. We estimated the contribution from this source is  $0.038 \pm 0.008$  in both search channels.

The reference channel is again  $B_d^0 \rightarrow K^+\pi^-$ . Monte Carlo events are used to calculate the relative reconstruction efficiencies between the search channels and reference channels. We obtain

$$\epsilon_{B_s^0 \rightarrow e^+e^-}^{rel} = 0.1290 \pm 0.0002 \pm 0.011$$

$$\epsilon_{B_d^0 \rightarrow e^+e^-}^{rel} = 0.1278 \pm 0.0017 \pm 0.011$$

where the first error is the statistical and second is the systematic error. The total systematic error of 8.9% includes uncertainties in  $dE/dX$  efficiency (4.8%), CEM fiducial coverage (2.0%), CES and CPR selection cut efficiency (3.0%), detector material counting (4.8%), track  $p_T$  threshold effect (2.7%),  $B_{s,d}^0$   $p_T$  spectrum in Monte Carlo (1.8%) and  $B_s$  lifetime uncertainty (3.0%).

Source	values	$\Delta\text{Br}(B_s^0 \rightarrow e^+e^-)$	$\Delta\text{Br}(B_d^0 \rightarrow e^+e^-)$
$N(B^0 \rightarrow K^+\pi^-)$	$6387.0 \pm 214.4$	3.4%	3.4%
$BR(B^0 \rightarrow K\pi)$	$(19.4 \pm 0.6) \times 10^{-6}$	3.1%	3.1%
$f_{B_d^0}/f_{B_1^0}$	$3.86 \pm 0.59$	15.3%	-
$\epsilon_{B_s^0 \rightarrow e^+e^-}^{Rel}$	$0.1290 \pm 0.011$	8.9%	-
$\epsilon_{B_d^0 \rightarrow e^+e^-}^{Rel}$	$0.1278 \pm 0.011$	-	8.9%
Total		18.3%	10.0%

Table 9: *Systematic uncertainties on the limits of  $Br(B_{s,d}^0 \rightarrow e^+e^-)$ .*

To calculate the branching ratio limits, we use the values and uncertainties listed in Table 9. Adding up the uncertainties gives a total systematic uncertainty of 18.3% for the  $B_s^0 \rightarrow e^+e^-$  search and 10.0% for  $B_d^0 \rightarrow e^+e^-$  as listed in Table 9. The results for different scenarios are listed in Table 10. Using the Bayesian calculation, we obtain the limits on the number of signal events of 3.11 (4.03) with 90 (95)% confidence level for the  $B_s^0 \rightarrow e^+e^-$  decay and 3.51 (4.47) with 90 (95)% confidence level for the  $B_d^0 \rightarrow e^+e^-$  decay. From this we calculate the limits on the decay branching ratios to be:  $Br(B_s^0 \rightarrow e^+e^-) < 2.8(3.7) \times 10^{-7}$  and  $Br(B_d^0 \rightarrow e^+e^-) < 8.3(10.6) \times 10^{-8}$  at 90 (95) % confidence level. In comparison, the best limit from  $B$ -factories is  $Br(B_d^0 \rightarrow e^+e^-) < 1.13 \times 10^{-7}$  [7] with 90% confidence level.

Search Channel	$N_{obs}$	$N_{bgr}$	Systematic uncertainty (%)	(BAYES)		(POILIM)	
				$N_{C.L.}^{90\%}$	$N_{C.L.}^{95\%}$	$N_{C.L.}^{90\%}$	$N_{C.L.}^{95\%}$
	no systematics, no background subtraction						
$B_s$	1	$0 \pm 0$	0	3.89	4.74	3.89	4.74
$B_d$	2	$0 \pm 0$	0	5.32	6.30	5.32	6.30
	systematics only						
$B_s$	1	$0 \pm 0$	18.3	4.23	5.24	4.10	5.08
$B_d$	2	$0 \pm 0$	10.0	5.47	6.50	5.41	6.43
	systematics and background subtraction						
$B_s$	1	$2.66 \pm 1.80$	18.3	3.11	4.03	3.33	4.27
$B_d$	2	$2.66 \pm 1.80$	10.0	3.51	4.47	4.15	5.16

Table 10: *Upper limits on signal events of  $B_{s,d}^0 \rightarrow e^+e^-$  from observed and estimated background events. Two programs (BAYES) and (POILIM) are compared and three background and systematic error conditions are shown. The systematic uncertainties are the summary of those affecting branching ratio calculations.*

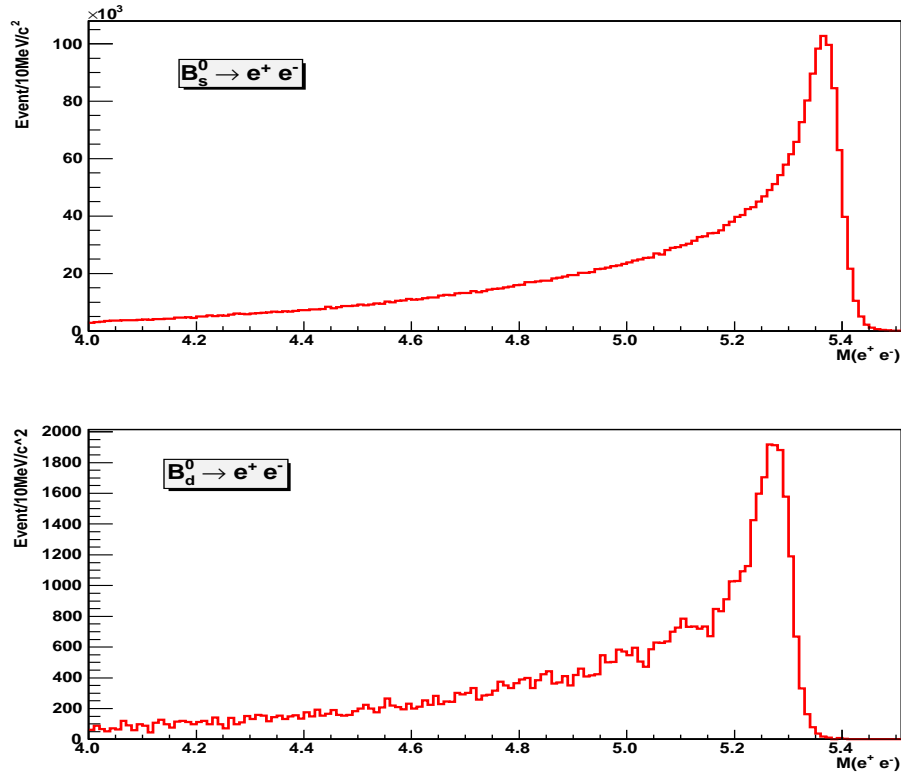


Figure 23: Monte Carlo invariant mass distributions for  $B_s^0 \rightarrow e^+ e^-$  and  $B_d^0 \rightarrow e^+ e^-$

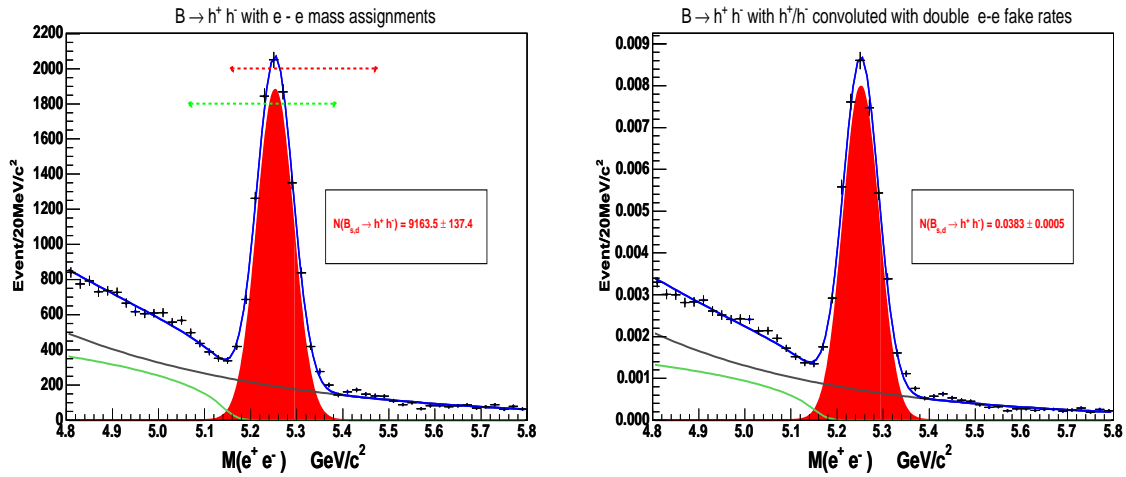


Figure 24: Invariant mass distribution of  $B_{s,d}^0 \rightarrow h^+ h^-$  events with electron mass assignments for the two tracks. The bottom plot is from events weighted by double electron fake rates.

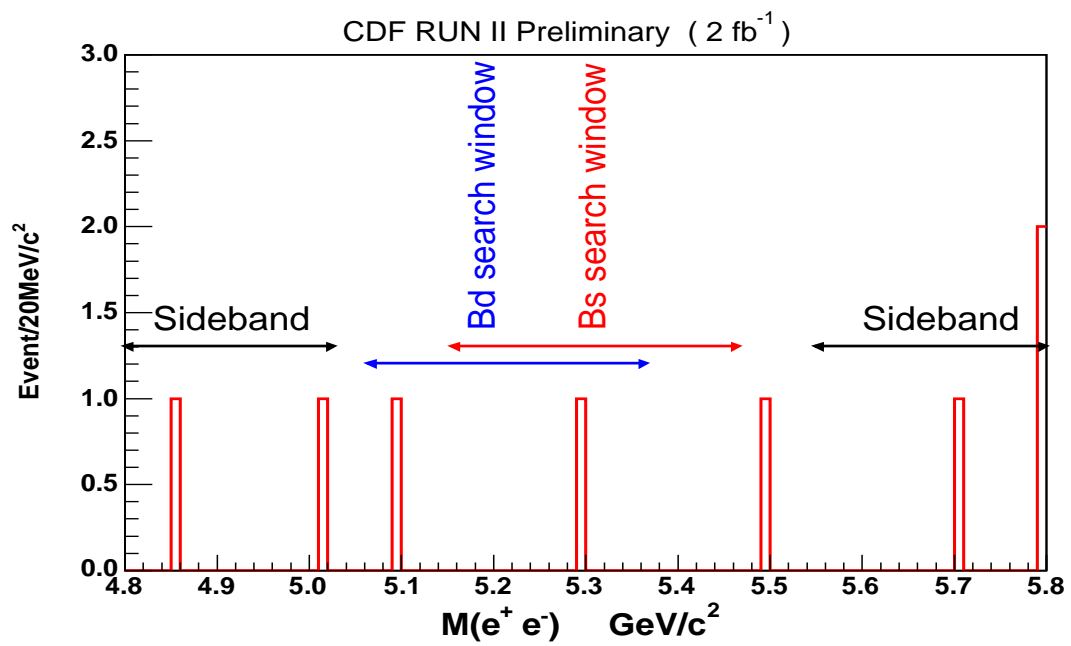


Figure 25: *Invariant mass distributions of the  $e^+ - e^-$  track pairs for events that passed electron identification.*

## 9 Summary

Using  $2 \text{ fb}^{-1}$  of CDF Run-II data, we perform a direct search for the lepton flavor violating decays  $B_{s,d}^0 \rightarrow e^+ \mu^-$ . We found no evidence of the decay in a sample collected by the two-track SVT trigger. Using the reference channel of  $B_d^0 \rightarrow K^+ \pi^-$  in which we reconstruct  $6387 \pm 214$  events in the same trigger sample, we derive the limits on the decay branching ratios

$$Br(B_s^0 \rightarrow e^+ \mu^-) < 2.0(2.6) \times 10^{-7}$$

$$Br(B_d^0 \rightarrow e^+ \mu^-) < 6.4(7.9) \times 10^{-8}$$

at 90(95)% confidence level. The corresponding lower bounds on the Pati-Salam leptoquark mass are:

$$M_{LQ}(B_s^0) > 47.7(44.6) \text{ TeV}/c^2$$

and

$$M_{LQ}(B_d^0) > 58.6(55.7) \text{ TeV}/c^2$$

at 90 (95)% confidence level. These results represent a significant improvement compared to CDF's previous measurement and the best result from B-Factories.

$$Br(B_s^0 \rightarrow e^+ \mu^-) < 6.1(8.2) \times 10^{-6} \text{ at } 90(95)\% \text{ C.L. (CDF 1998)[10],}$$

$$Br(B_d^0 \rightarrow e^+ \mu^-) < 9.2 \times 10^{-8} \text{ at } 90 \% \text{ C.L. (BABAR 2007)[7],}$$

$$M_{LQ}(B_s^0) > 20.7(19.3) \text{ TeV}/c^2 \text{ at } 90(95) \% \text{ C.L. (CDF 1998) [10],}$$

$$M_{LQ}(B_d^0) > 53.1 \text{ TeV}/c^2 \text{ at } 90 \% \text{ C.L. (BABAR 2007) [7].}$$

We also performed a search for the flavor changing neutral current decays  $B_{s,d}^0 \rightarrow e^+ e^-$ . We obtain:

$$Br(B_s^0 \rightarrow e^+ e^-) < 2.8(3.7) \times 10^{-7}$$

$$Br(B_d^0 \rightarrow e^+ e^-) < 8.3(10.6) \times 10^{-8}$$

at 90 (95)% confidence level. For the decay channel  $B_s \rightarrow e^+ e^-$  this is the first time a limit has been obtained. The result on  $B_d^0 \rightarrow e^+ e^-$  represents a big improvement over the 2007 BABAR result of  $Br(B_d^0 \rightarrow e^+ e^-) < 1.13 \times 10^{-7}$  at 90% confidence level which is currently the best from the B-Factories.

## Acknowledgment

The authors like to thank Giovanni Punzi, Michael Morello and Nicola Pounder for providing us with the mass fitting package and help on reconstruction of two-body B decay events TTT trigger, Stefano Giagu for help on techniques of offline confirmation of two-track trigger conditions, and Douglas Glenzinski for providing the Bayesian limit package. We also would like to acknowledge Robyn Madrak's involvement with this analysis in its early stage.

## References

- [1] J. Pati and A. Salam  
*Lepton number as the fourth "color"*, Physical Review D vol 10, Nr. 1, 275 Jul 1974.
- [2] R.A. Diaz, Eur. Phys. J. Cbf 41, 305 (2005).  
A. Ilakova, Phys. Rev. D **62** (2000).
- [3] G. Valencia, S. Willenbrock  
*Quark-lepton unification and rare meson decays*, Physical Review D vol 50, Nr. 1 Dec 1994.
- [4] M. Blanke *et al.*, JHEP **0705**, 013 (2007)
- [5] W. Marciano  
Physical Review D vol 29, 580 (1984).
- [6] The Particle Data Group  
W.-M. Yao *et al.*, J. Phys. G 33, 1 (2006) and 2007 partial update for the 2008 edition see WWW page: <http://pdg.lbl.gov/index.html>.
- [7] BARBAR Collaboration,  
SLAC-PUB-13040, Submitted to PRD (Dec, 2007);  
Physical Review Letter vol 94 (2005).
- [8] BELLE Collaboration,  
Physical Review D vol 68 (2003).
- [9] CLEO2 Collaboration,  
Physical Review D vol 62 (2000).
- [10] CDF Collaboration,  
Physical Review Letter vol 81, 5742 (1998).
- [11] Heavy Flavor Averaging Group: [www.slac.stanford.edu/xorg/hfag/ep-ex\\_0704.3575v1](http://www.slac.stanford.edu/xorg/hfag/ep-ex_0704.3575v1)
- [12] Heavy Flavor Averaging Group: [www.slac.stanford.edu/xorg/hfag/hep-ex\\_0603003](http://www.slac.stanford.edu/xorg/hfag/hep-ex_0603003)
- [13] R. Carosi *et al.*, CDF/ANAL/BOTTOM/CDFR/6356.
- [14] S. Donati, M. J. Morello, G. Punzi, D. Tonelli, G. Volpi, CDF note 8464, CDF note 8579,  
*Branching Ratios and CP asymmetries in  $B_{(s)}^0 \rightarrow h^+ h^-$  decays from  $1fb^{-1}$ .*
- [15] T. Moulik *et al.*, CDF internal note /CDF/ANAL/BOTTOM/CDFR/6793.

- [16] C. Campagnari *et al.*, CDF internal note /CDF/ANAL/TOP/CDFR/2161.
- [17] M. Aoki, I. Cho, S.Kim, T.Miao and I. Yu, CDF note 7518,  
*Measurement of  $B_c$  Cross Section Using  $B_c \rightarrow J/\psi e \nu$  Decay Channel.*
- [18] T. Moulik, CDF internal note /CDF/DOC/CALORIMETRY/CDFR/6192.
- [19] M. Riveline, CDF internal note CDF/DOC/CALORIMETRY/CDFR/5863.
- [20] Private communication with Vivek Tiwari on CPR2Q module.
- [21] S. D’Auria *et al.*, /CDF/PHYS/BOTTOM/6932 and the web page:  
”www-cdf.fnal.gov/internal/physics/bottom/COTDEDX/COT\_dedx\_cali.html”
- [22] S. Yu *et al.*, CDF internal note /CDF/ANAL/BOTTOM/CDFR/6361.
- [23] J. Bellinger *et al.*, CDF internal note /CDF/DOC/COMP\_UPG/CDFR/5870.
- [24] T. LeCompte, CDF note 6114,  
*Efficiency of Momentum Dependent Muon Matching Cuts.*
- [25] D.Glenzinski, M.Herndon, T.Kamon, V.Krutelyov, C.-J.Lin, J.Thom,  
CDF note 6835,  
*Kinematic-dependent matching cut for low- $p_T$  CMX muons.*
- [26] G. Punzi, “Optimization of searches for new signal”, physics0308063,  
www.arxiv.org/ps/physics/0308063.
- [27] Craig Blocker, John Conway, Luc Demortier, Joel Heinrich, Tom Junk, Louis Lyons, Giovanni Punzi, CDF note 7739, “ Recommendations Concerning Limits”.
- [28] Do-It-Yourself instructions for 6.1.4mc:  
www-cdf.fnal.gov/internal/physics/bottom/b-montecarlo/.  
This procedure uses BGEN to generate single B mesons using the  $p_T$  spectrum from the CDF Run-II measurement. EVTGEN is used to model the B-meson decays. SVT/XFT triggers are simulated using good runs listed in runlist\_614 (138809-212133).
- [29] E. Berry, I. K. Furic, R. Harr, Y. K. Kim, CDF note 8791.  
*Search for FCNC  $D^0 \rightarrow \mu^+ \mu^-$  Decays Using 360  $pb^{-1}$  of CDF Run II Data*
- [30] R. J. Hollebeek, P. K. Sinervo, H. H. Williams, CDF note 1109.